



This is a repository copy of *A pilot study into the geochronological and geomorphic context for the archaeology of Barrow Island, Western Australia.*

White Rose Research Online URL for this paper:

<https://eprints.whiterose.ac.uk/209680/>

Version: Accepted Version

---

**Article:**

Ward, I.A.K. [orcid.org/0000-0002-0566-1479](https://orcid.org/0000-0002-0566-1479), Bateman, M.D. [orcid.org/0000-0003-1756-6046](https://orcid.org/0000-0003-1756-6046), Larcombe, P. et al. (6 more authors) (2022) A pilot study into the geochronological and geomorphic context for the archaeology of Barrow Island, Western Australia. *Quaternary International*, 638-639. pp. 5-22. ISSN 1040-6182

<https://doi.org/10.1016/j.quaint.2022.02.002>

---

Article available under the terms of the CC-BY-NC-ND licence (<https://creativecommons.org/licenses/by-nc-nd/4.0/>).

**Reuse**

This article is distributed under the terms of the Creative Commons Attribution-NonCommercial-NoDerivs (CC BY-NC-ND) licence. This licence only allows you to download this work and share it with others as long as you credit the authors, but you can't change the article in any way or use it commercially. More information and the full terms of the licence here: <https://creativecommons.org/licenses/>

**Takedown**

If you consider content in White Rose Research Online to be in breach of UK law, please notify us by emailing [eprints@whiterose.ac.uk](mailto:eprints@whiterose.ac.uk) including the URL of the record and the reason for the withdrawal request.



[eprints@whiterose.ac.uk](mailto:eprints@whiterose.ac.uk)  
<https://eprints.whiterose.ac.uk/>

# **A pilot study into the geochronological and geomorphic context for the archaeology of Barrow Island, Western Australia**

Ingrid A. K. Ward<sup>a,\*</sup>, Mark D. Bateman<sup>b</sup>, Piers Larcombe<sup>a</sup>, Peter M. Scott<sup>c</sup>, Tanghua Li<sup>d</sup>, Kayla Murai<sup>e</sup>, Nicole S. Khan<sup>e</sup>, Peter Veth<sup>a</sup>, Patrick Cullen<sup>f</sup>

<sup>a</sup> Dept. Archaeology, School of Social Sciences, University of Western Australia, Australia

<sup>b</sup> Dept. Geography, Sheffield University, Sheffield, United Kingdom

<sup>c</sup> Oceans Graduate School, University of Western Australia, Australia

<sup>d</sup> Earth Observatory of Singapore, Nanyang Technological University, Singapore

<sup>e</sup> Dept. Earth Sciences and Swire Institute of Marine Science, University of Hong Kong, Hong Kong

<sup>f</sup> Dept Biodiversity Conservation and Attractions, Barrow Island, Australia

\* Corresponding author.

E-mail address: ingrid.ward@uwa.edu.au (I.A.K. Ward).

## **Abstract**

The island sanctuary of Barrow Island on the edge of the inner North-West continental shelf of Australia holds significant environmental as well as Indigenous and colonial cultural value. Insights on past occupation dynamics, particularly in response to Post-Glacial sea-level rise, continue to emerge from analysis of archaeological assemblages. However, there is limited temporal and landscape information from the wider island with which to better contextualise the physical site formation history of these cultural records. We present a new, modelled Post-Glacial sea-level curve for the region and new geochronological and sedimentological data (including rare earth element and quartz microtextural data) from non-archaeological site contexts to help infer changes in the coastal environment. This new data provides new insights on the island's paleogeography and evolution since approximately 80 ka BP in the context of inherited Last Interglacial features and highly dynamic oceanographic processes. Ongoing physical weathering processes have influenced dune building and reworking, such that neither colour nor numeric age are reliable indicators of sediment compositional and textural maturity. The results continue to emphasise how the continued integration of the island's geological, sedimentological and archaeological records help to understand aspects of cultural site formation, as well as expose some of the limiting factors in our understanding of past and present island dynamics.

**Keywords:** Geochronology; Geoarchaeology; Sea-level change; Barrow Island; Western Australia

## **1.0 INTRODUCTION**

Situated ~ 56 km off the Pilbara coast and on the seaward edge of the inner continental shelf, Barrow Island (20°45'S, 115°25'E) is one of the most important island sanctuaries in Western Australia. Its significance was recognised with its declaration in 1910 as a 'Class A' Nature Reserve (Moro and

Lagdon, 2013; see also Lynch et al., 2019). Additional significance came when a cave on the west side of the island was revealed to preserve evidence of human occupation dating back some 50 ka, and the earliest use of marine resources by modern peoples outside of Africa (Veth et al., 2017). Between 2013 to 2015 the *Barrow Island Archaeology Project* (BIAP) located 30 open surface sites and 20 caves and rockshelters, of which Boodie Cave is the largest (> 3000 m<sup>2</sup>). Conversely, the shell middens that are common in the coastal zone of the adjacent Onslow and Cape Range regions (Veth et al., 2014) are completely absent. A 2014 BIAP field report further noted the complete absence of prehistoric cultural materials from coastal dune, storm surge, and ‘tsunami’ deposits that post-date the stabilisation of Holocene sea levels.

Much can be gained from the study of the sediments that inform the past and contribute to the variable preservation of archaeological patterns across past landscapes (Karkanas & Goldberg, 2019). Currently, however, there is almost no geomorphic or geochronological data from the wider island and very limited regional sea-level data to contextualise the current findings and their broader archaeological significance. In other words, there is a limited temporal and physical context in which to understand these lived occupation records (Linse, 1993; Larcombe et al., 2018). This study was aimed at beginning to explore and date the non-archaeological contexts of Barrow Island, in particular the coastal dune sequences and inland clay pans associated with the main sites documented by BIAP (Figure 1). In addition, we undertook new sea-level modelling of the Post-Glacial rise in relative sea level (RSL) along this mid-shelf edge setting to help constrain changing oceanographic and sedimentary processes that have influenced coastal environments and available resources, as well as the nature and timing of the final stages of island formation.

## **1.1 Barrow Island**

### *1.1.1 Terrestrial Physical Environment*

The current physiography and environmental context of Barrow Island has been described by Hickman and Strong (2003) and Moro and Lagdon (2013) respectively, with a summary and bibliography provided by Smith et al. (2006). Boodie Cave and John Wayne rock shelter occur within the Trealla Limestone (Figure 2) that covers much of the North-West Shelf. The physiography of the island consists of areas of active erosion, particularly of the dissected limestone plateaux on the west side of the island, and areas of sediment accumulation in the form of shelly and calcareous aeolian dunes that parallel much of the island’s lowland coastline. The dunes’ colours range from pinkish-white dunes that are assumed to have formed with the establishment of modern sea level and hence are of Holocene age, to apparently older, redder dunes and sand plains (e.g., Benjamin et al., 2020). However, this association of colour and age has not been fully tested in the coastal Pilbara, and it is well known that colour can be influenced by a range of factors including parent rock, mineral and organic content and soil wetness (Lynn & Pearson, 2000; Pitts & Clarke, 2020).

Dune blowouts with scattered coral debris reflect the occurrence of past storms, whilst oyster-encrusted calcrete boulders and small boulders on the north-west and south-west coasts have been interpreted as deposits of past tsunamis (Playford, 2014). Inland and eastward, the gently undulating rocky terrain and inland claypans change to dune systems and fringing mangroves nearer the coast (Moro and Lagdon, 2013). There are thus a wide array of sedimentary processes, environments and deposits, the systematic study of which can help provide an understanding of the processes that allow links to be made between site-specific archaeological records and their broader geological or geomorphic landscape setting.

### *1.1.2 Past Relative Sea-Level (RSL) Changes*

Past RSL changes for Western Australia (WA) in general, and especially for the Pilbara shelf, are poorly constrained by field observations (Lewis et al., 2013), with almost no sea-level data of quality constraining past elevations between 100 and 25 m below modern RSL (Figure 3). The earliest work was reported by Fairbridge (1961, his fig. 2) who used the bathymetric observations of Carrigy and Fairbridge (1954) to propose several stillstands in the Post-Glacial rise in RSL. Interpreted as sea-level indicators, horizontal terraces occurred at depths of 101, 74, 64, 37, 18 and 2 m below modern sea level (inset Figure 3), found at the same depths around islands on the shelf, and on the open shelf itself, taken as indicating relatively little crustal flexure across and along the shelf. Eisenhauer et al. (1993) used coral cores from the Abrolhos Is., 1000 km to the south, to interpret that the rising sea level passed through ~ -24 m at about 9.8 ka (U/Th age) and first rose above the present level at 6.3 ka (U/Th), and that a high mid-Holocene RSL persisted to at least ~4.7 ka before falling. More recently, Lessa & Masselink (2006) interpreted the elevation of the mid-Holocene highstand to be ~1 m above modern levels at 2.7 ka, based on stratigraphic evidence just north of Broome, 800 km to the NE.

These and related sea-level data have been used by various regional archaeological (e.g., Hook et al., 2004; Veth et al., 2007; Ward et al., 2014) and more general studies (Moro & Lagdon, 2013) of the Barrow area. To date, little account has been taken of associated sedimentary processes that may affect preserved sea-level constraining points, and which may be associated with periodic drivers like tidal currents or seasonally large waves, episodic drivers like tropical cyclones, or longer-term fluctuations in rainfall and river discharges associated with climatic variability.

### *1.1.3 Climate and Oceanography*

Barrow Island lies on the southern margin of the zone of tropical precipitation associated with the Indo-Australian summer monsoon (IASM) and the northern margin of the zone of extratropical precipitation associated with the Southern Hemisphere westerly winds (SHWW). Stalagmite records from Ledge Cave on Barrow Island, obtained as part of the BIAP reveal greater IASM variability and wetter conditions prior to human arrival on the island within Marine Isotope Stage (MIS) 4 (82–71 ka), followed by a significant drying phase and cessation of growth of the Ledge Cave stalagmite

starting at approximately 60 ka (MIS-3; Conningham, 2017). Isotopic studies of mammal teeth from Boodie Cave further show a shift towards increasing aridity in the period 36.6–46.2 ka, preceding the onset of the Last Glacial Maximum (LGM) and a period of increased humidity in the early to mid-Holocene (7.2–6.8 ka BP; Skippington et al., 2021).

The current climate is more arid - subtropical, with summer rainfall the result of tropical cyclones associated with the IASM and winter rainfall delivered by the SHWW. Rainfall is heavily dependent on rain-bearing low-pressure systems and the passage of tropical cyclones, with a mean annual rainfall of 320 mm (Chevron, 2005). Mean annual maximum temperatures are 29°C, with summer temperatures of up to 45°C and correspondingly high evaporation rates of 3,500 mm/yr (Chevron Australia, 2005). Creek flows are at best seasonal or are dormant, and the presence of surface water in the claypans is rare and ephemeral. Non-cyclonic winds are strongly seasonal. In winter, a subtropical ridge moves north bringing dry easterly and south-easterly winds (6–8 m/s) and moderate north-westerly winds (10–13 m/s) in the summer months. The region experiences an average of five cyclones per year, at least two of which make landfall. Under extreme cyclone conditions winds can reach 180 km/hr (Condie et al., 2006).

Tides in the Barrow Island region are semi-diurnal and have a maximum range of just over 3 m at spring tides, which combined with the shallow bathymetry on the east side of the island, results in expansive areas of exposed seabed at low tide. Tidal currents are strongest in the narrow passage between Barrow Island and the Montebellos, and through the Mary Anne Passage between Barrow Island and the coast. Retrodictive modelling indicates that tidal ranges and currents in the region are likely to have significantly changed over the past 20 ka with changing shelf configurations associated with sea-level rise (Ward et al., 2013).

#### *1.1.4 Coastal Processes*

Barrow Island lies on a limestone shelf that also underlies the Montebello Islands. To the west, the rugged coast and narrow intertidal zone grades sharply to the limestone middle shelf, whereas to the east and south, broad intertidal areas give way to a shallow limestone shelf, with depths generally less than 20 m. The Pilbara shelf and coastline has been influenced by a wide variety of past and present driving processes that influence the formation of coastal environments and the timing of island formation. In winter, the dry easterly and south-easterly winds drive shelf waters towards the west, and in summer winds tend to drive shelf waters gently eastwards. Cyclones can force fast unidirectional currents on the shelf (Pearce et al., 2003) with 17 m high ocean waves and surface ocean currents exceeding 3 m/s (Condie et al., 2006). Over periods of decades and centuries, the fastest cyclone-driven flows are towards the SW, in the same direction as along-shelf sediment transport (Larcombe et al., 2014, 2018; Dufois et al., 2017). Cyclones can also raise water levels well beyond normal tidal levels, cause coastal erosion and drive sediments inland. There is a variety of

geological evidence of past large tsunamis in the region (Playford et al., 2013; Playford, 2014). Historical evidence for minor tsunamis originating in Indonesia is well documented (Dominey-Howes, 2007), and this is also known for the Holocene (Scheffers et al., 2008).

Hence there are a variety of relevant oceanographic processes involved in assessing the mobility of sediments, development of coastal environments and potential reworking of archaeological artefacts from primary to secondary depositional contexts in the region over the last 10,000 years or so, more broadly over the Post-Glacial transgression, and for the preceding periods.

At present, Barrow Island is starved of terrigenous sediment, with little physical erosion on the island itself, and the shelf surrounding it consists largely of patchy highly mobile calcareous sands and gravels overlying cemented calcarenite (Chevron Australia, 2005), with corals in places especially on the eastern side. A wide variety of submarine bedforms formed of bare sand and gravel are especially prominent to the south near the Barrow Island Shoals and towards the mainland - active bed sediment transport is indicated at all timescales (Larcombe et al., 2014; Lebrec et al., 2021). Tidal currents and waves move sands every day, and large gravel bedforms indicate episodic transport from fast currents, probably associated with cyclones. Sediments now accumulate near the coast only in very small areas and probably only ephemerally, such as in western Bandicoot Bay (see location in Figure 2) at the island's southern end. The low rates of terrigenous sediment supply, long periods of weathering and abrasion, combined with the dynamic coastal environment are likely to have promoted the preferential accumulation of available heavy minerals in some areas.

#### *1.1.5 Archaeology*

Several pre-development palaeontological and heritage mitigation studies have been undertaken on Barrow Island (e.g., Hook et al., 2004; Kendrick & Mau, 2003; McNamara & Kendrick, 1994; see also Souter et al., 2006 and references therein). These studies noted the presence of open sites, especially on the claypans in the south of the island, and the possibility of cultural deposits in stratified (cave and rock shelter) sites. This was followed by the BIAP project, which resulted in the documentation of colonial era (c. 1880–1900) pearling and maritime sites of Bandicoot Bay and South End (Figure 2; Paterson, 2017; Paterson & Veth, 2020; Byrne et al., 2020), and the much older, late Pleistocene to early Holocene sites of Boodie Cave (Figure 2; Veth et al., 2017; Ward et al., 2017; 2018) and John Wayne rockshelter (Figure 2; Ditchfield et al., 2018), as well as 30 open site artefact scatters, of variable size and composition, on the island (Figure 2; Zeanah et al., 2014; Ditchfield, 2018).

The Late Pleistocene-age cave and rockshelter sites on Barrow Island are dominated by artefacts manufactured from local limestone (Ditchfield et al., 2018; Veth, 1993; Veth et al., 2007; 2017) while undated surface scatters tend to be dominated by non-local lithologies (Ditchfield & Ward, 2019). Some calcareous artefacts may have been sourced from a silicified limestone 'quarry' site on the

northern tip of the island (Figure 2B; Ditchfield, 2018). Exposures of white and red silicified limestone outcrops had been quarried, with defined reduction areas with rotated cores, flakes and debris in association (Figures 2C). These features were mapped in detail by BIAP and will be published as a separate site report (Zeanah et al., in prep). The quarry site is now situated within a large dune blowout, with laminar calcrete exposed around basal edges of weathered reef mounds and as linear (NNW-SSE) deposits, surrounded by dunes up to 6 m high. There are no absolute dates for any of the open sites, but the non-local artefacts are assumed to have been derived from the mainland and hence to relate to the period before Barrow became an island.

A series of surface shell scatters of the mangrove gastropod *Terebralia palustris* were identified by Pat Cullen in November 2015 near the Wapet Landing (Figure 1 and 8). The scatter comprises three main clusters, each 5–30 m in diameter, of sparse, fragmented shells, of which the most southerly scatter is the largest. The shells are mainly *Terebralia* sp., with whole shells measuring 3–8 cm in length and representing both juvenile and adult stages. Similar scatters, composed entirely of *Terebralia* sp. and coral grit, were recorded directly above a beach by Veth and colleagues on the Montebello Islands in 1992 and 1994 and were investigated using test pits (Veth et al., 2007). These investigations confirmed a monospecific composition yet variable size range, inclusion of coral and abraded shell fragments and complete absence of charcoal and stone artefacts, from which it was concluded that these were storm-reworked shell bed or chenier deposits (Veth et al., 2007). While the Wapet Landing shell scatter has not had a comprehensive archaeological site inspection it does have a similar monospecific composition and variable size range, and is included in the current geoarchaeological study of non-archaeological site deposits on Barrow Island.

## **2.0 METHODS**

### **2.1 Fieldwork**

Two 5-day fieldtrips were undertaken, the first a reconnaissance trip in April 2019 and the second a dedicated sampling trip in September 2019, focussing mostly on the five areas noted above. A red, quartz-rich dune in the northeast of the island (Figure 2 and 7), unusual because the island's dunes are otherwise almost entirely composed of biogenic carbonate, was also sampled. Collected sediment samples were analysed for particle size distribution (PSD) to help characterise the sediments at the University of Western Australia (UWA), using a Malvern Mastersizer 2000, except for one sample, BIQ19\_3, which was measured using a Horiba LA-950 laser diffraction particle size distribution analyser at Sheffield University.

Deposits were sampled for optically-stimulated luminescence (OSL) dating around the quarry site (sample name BIQ, Figure 4), Loop Beach (The Chair, sample BIC, Figure 5), on the red dune (sample BID, Figure 6) and on the face of the exposed drill-pad (sample BIGP, Figure 7). At the

quarry site, dune deposits were excavated on the north (Site 1 and 2) and south side (Site 3) to depths of 4 m and 1.2 m respectively (Figure 4). Horizontal bedding visible on exposed wind-blown surfaces of the dune provided some confidence that sampling was in intact dune sediment rather than any slumped material. Sampling of these larger deeper dunes was achieved using a Dormer Engineering sand auger, fitted with a special OSL sample collection tube to collect unexposed sediments at depth. For the smaller dunes on the north side of the quarry, sampling was achieved by exposing a face into which a steel tube was pushed or gently hammered. A sample of laminated calcrete, overlying older, cemented reef deposits, was also collected at the quarry site for U-series dating analysis.

Dunes of different colours were sampled either side of a creek at Loop Beach (The Chair) by similarly pushing a steel tube into an exposed face of the creek or excavated dune profile. This same sampling method was used for the quartz-rich red dune. Although artefact scatters had been recorded on the surface of several of the dry claypans, these shallow, fine-grained deposits were extremely hard-packed and difficult to sample. An exposed drill-pad from a nearby gravel pit (BIGP) was taken to represent equivalent deposits, around which isolated artefacts – likely reworked – could still be found (Figure 7). Sampling of an exposed face of drill-pad was similarly sampled using a steel tube above the gravel – clay interface at 51 cm.

In addition, a large fragment (~ 2 cm across the aperture) of a *Terebralia* sp. shell was collected from the exposed drill-pad face at 30 cm depth for radiocarbon dating. This, and the few other similarly large *Terebralia* sp. shell fragments, were not considered to be cultural because of their size (inedible) and likely had been naturally reworked with the surrounding sediments. A single *Terebralia* sp. shell sample was also collected from the shell feature near Wapet Landing (Figure 8). Shells were submitted to Waikato radiocarbon lab for dating by AMS analysis. Samples for OSL dating were taken to Sheffield University for processing and analysis.

## **2.2 Laboratory analyses**

### *2.2.1 Radiocarbon analysis*

The two *Terebralia* sp. shells (Wk-503029 and Wk-503030) were analysed using standard Accelerator Mass Spectrometry (AMS) at Waikato, New Zealand. Dates were calibrated using the Marine20 curve (Heaton et al., 2020) and a regional  $\Delta R$  of  $109 \pm 25$   $^{14}\text{C}$  years for marine samples (Veth et al., 2017). Results are provided in Table 1.

### *2.2.2 Laser Ablation U-series age screening dating*

Laser ablation (LA-) U-series age screening was performed at the Advanced Geochemistry Facility for Indian Ocean Research at the University of Western Australia. In brief, a Teledyne Analyte G2 laser ablation (LA-) setup is coupled to a Thermo-Fisher NEPTUNE+ MC-ICP-MS using an approach

modified after Scott (2019) and Spooner et al. (2016). Repeats with any evidence of detrital contamination (using  $^{232}\text{Th}$  as a proxy) were discarded. Instrumental biases were corrected relative to a secular equilibrium carbonate of known isotope composition, and two secondary standards ( $n=7$ ;  $n=7$ ) yielded accurate, under-dispersed, results for  $\delta^{234}\text{U}$  ( $\pm 40\%$ ) and ages ( $\pm 2.5\%$ ). It is worth noting that this approach is referred to as an ‘age screening’ method rather than a ‘dating’ method – this is to reflect the lower precision compared to ‘conventional’ solution U-series measurements. Full results are provided in Supplementary Table S1.

### 2.2.3 OSL dating

The total environmental dose rate for each sample was measured by inductively coupled plasma mass spectrometry (ICPMS) at SGS laboratories, Ontario Canada (Supplementary Table S2). Elemental concentrations were converted to annual dose rates using data from Guerin et al. (2011), accounting for attenuation factors relating to sediment grain sizes used, density and palaeo-moisture. The contribution to dose rates from cosmic sources was calculated using the expression published in Prescott & Hutton (1994).

Single-grain OSL dating was applied to fine sand quartz grains (size fraction 180–212  $\mu\text{m}$ ) extracted from eleven samples as per Bateman & Catt (1996). Equivalent dose ( $D_e$ ) values were obtained using the single aliquot regenerative-dose (SAR) procedure (Murray & Wintle, 2000; 2003), which included standard tests of signal suitability (e.g., recycling ratio, recuperation, and OSL-infrared (IR) depletion ratio (Duller, 2003)). Preheats of 260°C for 10 seconds were applied to OSL measurements to remove any unstable signal generated by laboratory irradiation. For each sample, up to 1200 grains were measured, of which ~10% passed the acceptance criteria. Some samples contained some saturated and zero-dosed grains and non-normal  $D_e$  replicate distributions – these are assumed to have been pedoturbated (see Bateman et al., 2003; 2007) and/or partially bleached prior to burial or during sampling. Whilst attempts to mitigate this have been made using the Finite Mixture Model, the resultant reported ages may still be impacted by this and should be viewed in this context. Final age estimates reported from the year 2020 with 1-sigma uncertainties are presented in Table 2 and discussed for each site area below.

### 2.2.4 REE analysis and quartz microtextural analysis

Element concentrations, collected as part of the ICPMS analysis at Sheffield University for environmental dose rate calculations and in previous OSL analyses for BIAP by Oxford University, can also be explored for all the dated dune and claypan samples. This previously unpublished data relate to OSL samples collected within excavation profiles from Boodie Cave (Veth et al., 2017) and John Wayne rockshelter (Ditchfield et al. 2018). Rare Earth Elements (REE) occur in more resistant phases, especially heavy mineral phases, including zircon ( $\text{Zr}(\text{SiO}_4)$ ), rutile ( $\text{TiO}_2$ ) and ilmenite ( $\text{FeH}_6\text{O}_3\text{Ti}$ ) hence are particularly useful to assess palaeoenvironmental source and weathering. REE

may also form part of the chemical structure of phosphate minerals monazite ((Ce,La,Nd,Th)(PO<sub>4</sub>,SiO<sub>4</sub>)) and xenotime ((Er, Ce)(YPO<sub>4</sub>)). Hence just as heavy mineral abundance can be used to differentiate age of dune deposits (Tapsell et al., 2003), REE concentrations can provide an indication of sediment compositional maturity. Elemental abundances also exist from previous OSL dating analyses from Boodie Cave (Veth et al., 2017; Ward et al., 2017) and one open site in the NE of the island (Ward et al., 2016). The available geochemical data from these ICPMS analyses was limited for the Boodie Cave samples but common data were available in the both the light (LREE; La, Ce, Pr, Nd, Pm, Sm, Eu) and heavy rare earth elements (HREE; Dy, Gd, Ho, Lu, Tb, Tm, Yb) (Supplementary Table S3).

Quartz, as another resistant mineral, can also be used to explore palaeo-environmental and weathering trends (Vos et al., 2014). Quartz grains from all the dated dune samples were separated by digesting the carbonate-rich sediments in 10% hydrochloric acid until all fizzing ceased, and the residue was washed and decanted several times in water before oven drying at 40°C. This method retained coatings and/or adhering particles that might inform of past diagenesis (see Vos et al., 2014). Quartz grain morphology and micro-texture was profiled using a JEOL Neoscope SEM, the latter housed at the Centre of for Microscopy, Characterisation and Analysis at UWA.

### **2.3 Modelling of Relative Sea-level (RSL)**

New relative sea-level (RSL) curves were computed for this specific area (20°45'S, 115°25'E) using Glacial Isostatic Adjustment (GIA) models. We used two state-of-the-art ice models: ICE-7G\_NA (Roy & Peltier, 2017, 2018) and that developed at the Australian National University by Kurt Lambeck and collaborators, hereafter referred to as ANU-ICE (e.g., Lambeck & Purcell, 2005; Lambeck et al., 2014; 2017). We used the 3-D earth model HetM-LHL140 (Li & Wu, 2019) to couple with both ice models in this study. The parameters of the 3-D earth model were tuned to achieve the best fit with GIA-related observational data in North America and Fennoscandia when fixed with ICE-6G\_C (e.g., Peltier et al., 2015) ice model (Li et al., 2018; Li & Wu, 2019).

RSL data were compiled from published radiocarbon and OSL ages from coral reefs, tidal flats and sand ridges from Exmouth Gulf and the Ashburton Delta (May et al., 2015; 2016; 2018; Twigg & Collins, 2010). These have been assumed to share a sufficiently relatively similar RSL history and influence from processes such as hydro-isostasy to Barrow Island (Lambeck, 2002; Nakada & Lambeck, 1989) for the purpose of this paper. We followed internationally established standard protocol to estimate the RSL, age, and associated vertical and temporal uncertainty for each sample (Hijma et al., 2015; Khan et al., 2019). As noted above (section 1.1.2), there are few data in the eastern Indian Ocean and around Australia to ground truth these models, and no data at all in WA between -95 and -30 m. The published record begins at 8.1 ka, where an index point places RSL at -6.4 ± 0.2 m. See Supplemental section 1.1 for more details of the RSL modelling.

## 3.0 RESULTS

### 3.1 Relative Sea-level (RSL)

The calculated RSL curves are presented in Figure 3. Differences between the two RSL curves are attributed to the different deglaciation history (i.e., ice-equivalent sea level) they employed, mainly caused by i) different methods of solving the sea-level equation (e.g., Lambeck et al., 2017; Roy & Peltier, 2017) and ii) different sets of external geological and geophysical constraints (e.g., RSL data, GPS data) (e.g., Lambeck et al., 2014; Peltier et al., 2015). We have differentiated between pre-Holocene and Holocene marine limiting data because for the pre-Holocene deglaciation the hydro-isostatic effects are likely to be less variable across and along wider areas of the shelf and differences are less important than for the Holocene. Despite the discrepancy between the two curves (Figure 3), both are helpful in indicating the likely limits and ranges of the deglacial RSL history for this region, and thus in informing the geological development of Barrow Island.

### 3.2 The silicified limestone quarry (BIQ)

#### 3.2.1 Sediment description

The dune sediments on the north side of the quarry are uniformly pale pink (2.5YR 7/2), moderately sorted, coarse sands (520 - 580  $\mu\text{m}$ ), mostly comprising biogenic carbonate grains (89 – 90 %) with lesser sub-prismoidal quartz (10 – 20%). Sediments increase downcore in moisture, hence also depth of colour, and in their compaction. At the very base of the dune, at the interface with the quarry pavement, the well-compacted, dark red (2.5YR 5/6) sand grains were finer and more spherical, comprising medium sands ( $\sim 350 \mu\text{m}$ ) with a greater fine-sand component, and much lower carbonate content ( $\sim 45\%$ ; Figure 4).

#### 3.2.2 Chronology and geochemistry

OSL ages indicate that these pink dune sediments are all younger than 1600 years old (Table 2; Figure 4). These results indicate rapid net accumulation rates of 2 – 9 m/ka. The age of the underlying well-compacted, dark red sands is estimated at  $7.6 \pm 0.44 \text{ ka}$ , giving a net accumulation rate of 3 cm/ka. The shallower dune sediments on the south side of the quarry were also dark red (2.5YR 5/6) and coarse ( $\sim 330 \mu\text{m}$ ) but largely unconsolidated, and dated to  $1.22 \pm 0.17 \text{ ka}$ , again giving a rapid net accumulation rate of 0.7 m/ka. Accumulation here is likely to be episodic rather than continuous.

OSL ages of sand found between calcrete bands within the quarry floor deposits indicates an age of at least  $75 \pm 5.6 \text{ ka}$  (Table 2). This corresponds excellently with the LA-U-series weighted mean age of  $74.1 \pm 4.2 \text{ ka}$  ( $n=9$ , MSWD=3.1) determined from nine 1 mm line rasters along the  $\sim 4 \text{ cm}$  length of the cream-coloured laminae (Figure 4). The calculated initial uranium isotope composition ( $\delta^{234}\text{U}_i$ ) of  $313 \pm 19\%$  ( $n=9$ ) is elevated relative to marine values, suggesting the involvement of pore fluids/groundwaters in precipitation of the calcite layer. An alternative interpretation of the elevated

$\delta^{234}\text{U}_i$  value could be open-system behaviour (post deposition mobility of U and/or Th) but is considered unlikely given the consistency of replicates across the area of the sample. The significance of the calcrete age estimates is discussed below.

Individual REE concentrations generally show a positive correlation with OSL ages (Figure 10; see also Supplementary Figure S1). For the quarry samples alone, the highest REE and highest zircon concentrations occur in the older red sands at the base of the quarry but are not significantly high compared to other dated samples (Table S2). These sediments also have high Al, Ti, K and Fe, Mn values reflecting high clay and oxide contents respectively. A high ratio of Fe/K (> 4), K/Ti (> 10), comparatively high Th/U (> 1) (Table 3) and enrichment of LREE over HREE (Figure 10) is also indicative of intense physical weathering of these older sediments.

### 3.2.3 *Quartz grain morphology*

Within the younger dune sands (e.g., BIQ19-1), the quartz morphology is generally low to medium sphericity, sub-rounded to sub-angular and of medium to high relief, with a mixture of shiny and dull grains (Figure 9a). Mechanical microtextures include meandering ridges and straight grooves (e.g., Figure 9c and d) and abundant crescentic marks (< 100 $\mu\text{m}$ ), and bulbous edges on more rounded grains (e.g., Figure 9c). Chemical weathering features include orientated etch pits (e.g., Figure 9d), triangular and rhomboidal solution pits, and solution crevasses. The latter are more abundant in the more angular grains.

In contrast, the morphology of quartz within the older, red sands at the base of the quarry dunes (BIQ19-4) tend to be slightly more spherical, sub-rounded, and of medium relief (Figure 9e). The flat, pitted surface of the grains are covered by a veneer, with adhering particles (mainly clays) and chemical precipitation in depressions (e.g., Figure 9f). V-shaped features are completely absent. Older conchoidal fractures and meandering ridges (e.g., Figure 9h) are evidence of previous mechanical weathering.

## 3.3 **Loop Beach (The Chair, BIC)**

### 3.3.1 *Sediment description*

The creek base (~ 1.5 m ASL) was composed of consolidated reef deposit – assumed to be sensu lato last interglacial in age based on elevation, with large (decimetre size) remnant corals and shells. The surrounding mobile dunes were up to 9 m above sea level, with samples taken from the red sands lying unconformably beneath pink sands on the south of the creek (Site 1), and by excavation from pink sands on the landward (Site 2) and seaward (Site 3) side of the dunes on the north side of the creek (Figure 5).

These dune sediments comprised pink (5YR 7/3), moderately-sorted, coarse (~ 640  $\mu\text{m}$ ) sands, mostly comprising biogenic carbonate (95 %) with minor sub-prismoidal quartz (5%). The dark red sediments (2.5YR 4/6) at the base of the creek profile comprised semi-rounded to semi-angular grains, with a slightly smaller modal grains size (~ 445  $\mu\text{m}$ ) and slightly lower carbonate content (85%) than the overlying pink/white sands. The landward dunes were much coarser (~ 1170  $\mu\text{m}$ ) but still with abundant prismoidal shell and coral fragments. Although similar to the beach sands, grains of the coastal dunes are notably more abraded and less polished.

### 3.3.2 *Chronology and geochemistry*

The OSL age estimates from all these dunes were relatively young, ranging from  $2.2 \pm 0.18$  ka in the more landward dunes to  $< 900 \pm 140$  yrs in those more seaward. The youngest age estimate of  $\sim 120 \pm 20$  yrs (using central age model) was from the dark red sediments (BIC19-1) at the base of the creek profile, and seems anomalously young given their colour and thick (<9 m) overburden of white sand. Even using a finite mixture model for poorly bleached/pedoturbated samples with overdispersion, only 2% of the data would give an age older than 2.5 ka, which is still young. The young age indicates that there has been some reworking of the red sands, perhaps as creek runoff or as slumping. Net vertical sediment accumulation rates in these dunes range from 0.4 to 1.7 m/ka, which together with the ages, indicate episodically mobile dune sediments.

REE concentrations again show a positive correlation with OSL ages, except for sample BIC19-1 from the base of the creek profile. These dark red sediments have the highest total LREE abundance relative to age (Figure 10) and the second highest REE concentrations of all dated samples, slightly higher than red sediments from the Quarry (BIQ19-4-1) that provided an age of  $7.6 \pm 0.44$  ka (Table 2). The higher LREE/HREE ratio imply a higher level of sediment maturity that is at odds with the young OSL ages for BIC19-1. Additionally, geological source indices, including Zr/Hf and Cr/Th, are significantly lower, and weathering indices, including as Th/U, Rb/Sr and Ba/Sr, are significantly higher for BIC19-1 compared to the other dune samples from this location (Table 3). Hence it is possible that the BIC19-1 sediments derive from a different source; possibly leached limestone or claypan deposits. Additional geochemical sampling of the limestone bedrock and any associated saprolite deposits are needed to confirm this.

### 3.3.3 *Quartz grain morphology*

The sampled quartz grains from the red dunes (BIC19-1) are typically of medium sphericity, sub-rounded to sub-angular, and of medium relief with bulbous edges (Figure 9l). The red clay coating is visible under SEM as a smooth solution surface and adhering particles. Abrasion fatigue (e.g., Figure 9k), meandering ridges and intense chemical precipitation in grooves and depressions (e.g., Figure 9l) are consistent with an aeolian palaeoenvironment (Vos et al., 2014), with crystal overgrowth

indicative of diagenesis in carbonate-rich sediments (Ramos-Vazquez & Armstrong-Altrin, 2020). As for the red sediments at the quarry, v-shaped features are absent.

For the pink/white dunes at Loop Beach (e.g., BIC19-4), the morphology of the quartz grains is more variable and includes angular to sub-rounded grains of medium sphericity and variable relief (Figure 9m). More angular grains show clear pitted surfaces and orientated etch pits indicative of sub-aqueous conditions (e.g., Figure 9n), whilst more rounded grains show bulbous edges, smooth-surfaces with abundant (not oriented) v-shaped grooves (e.g., Figure 9p) indicative of more littoral environments.

### **3.4 The red dune (BID)**

#### *3.4.1 Sediment description*

In marked contrast to the western side of the island, the dark red (2.5 YR 3/6) dune sediments sampled on the northeastern side of the island comprise almost pure quartz. The sands are distinctly coarse unimodal (mode 520  $\mu\text{m}$ ), and both rounded and spherical in shape. The same unimodal profile is shown in sands (NT2 - NT5) taken in a short coastal transect approximately 2 km to the south of the Quarry site on the NW of the island. Despite their deep red colour, when etched in HCl the quartz grains of the red dune are very dull and show little or no red colouration (in contrast to BIC19-1 and BIQ19-4). Nevertheless, ICP analyses indicate very high concentrations of Fe and Ni in these red sands, indicative of lateritic weathering, and very low concentrations of U, which also is indicative of leaching (Table 3).

#### *3.4.2 Chronology and geochemistry*

Despite their apparent compositional and textural maturity, OSL ages return an age of only  $1.88 \pm 0.14$  ka (Table 2), indicating these quartz-rich sands are recently reworked. The low carbonate content of these sediments is reflected in the high ratio of Rb/Sr (or very low Sr values). Similar dark red, quartz-rich (> 60% SiO<sub>2</sub>) sediments of the same modal grain size (~520  $\mu\text{m}$ ) occur from low dune and palaeosol sediments in the north of Barrow Is. and may represent remnants of older facies that continue to be reworked and mixed with more recent, carbonate-rich sediments particularly around the island's coast.

Concentrations of Al, Ti, K, Fe, Mn are moderately high, reflecting contribution of clays and iron oxides to the red colouration of these sands. Concentrations of Zr (98 ppm), Th (2.2 ppm) and REE, especially LREE (~ 21 ppm), are only moderately high and reflect a less intense weathering compared to the red sediments from the dunes (BIC19-1 and BIQ19-4) or the gravel pit (BIGP19-1) (Supplementary Table S3). However, like the red sands from Loop Beach and the Quarry, the quartz-rich red dunes do show a high abundance of LREE relative to their absolute age (Figure 10).

### 3.4.3 Quartz grain morphology

The grains of the red dune are typically rounded to sub-rounded, of med-high sphericity and medium to high-relief (Figure 9q). Common grain micro-textures include crescentic marks (e.g., Figure 9r), v-shaped gooves (e.g., Figure 9s), straight steps and occasional chattermarks (e.g., Figure 9t). Chemical microtextures include triangular and occasional rhomboidal solution pits.

## 3.5 The drill-pad claypan (Fonz' gravel pit, BIGP)

### 3.5.1 Sediment description

Located ~ 6.8 m ASL, the sediments in the claypans inland from Loop Beach are typically dark reddish brown (2.5 YR 3/4) to weak red (10R 4/4) poorly sorted sands, comprising relatively quartz-rich clayey sands (~50%) mixed with very coarse sub-angular limestone fragments. The drill pad face shows deep-red, fine sands unconformably overlying a gravel unit (Figure 7). A few *Terebralia* sp. shell fragments occurred in the upper unit (Figure 7).

### 3.5.2 Chronology and geochemistry

Radiocarbon dating of a *Terebralia* sp. buried at 30 cm depth provided an age estimate of 11,876 – 11,359 cal BP (Wk-503029). The OSL dating indicated a mixed age of  $7.39 \pm 0.59$  ka (29%) and  $14.11 \pm 0.97$  ka (57%) (Table 2), providing a net accumulation rate of 4 – 7 cm/ka. These sediments show the highest concentration of Al, Ti, Fe and Mn (Table S2) reflecting the higher concentration of fine, ferruginised sands and clays that make up these deposits. They also have the highest concentrations of REE and Zr (302 ppm) and highest ratio of Th/U (7.2) and Fe/K (7.0) (Table 3) indicating both intense weathering and the concentration of resistant phases in these claypan deposits. The older of these age estimates is more consistent with the high concentration of REE and is plotted as such in Figure 10.

## 3.6 Wapet shell feature

A single *Terebralia* sp. shell was radiocarbon dated at 7,563–7285 cal BP (Wk-503030). Whilst the shell feature is not considered to be cultural, this age indicates the early Holocene presence of mangroves, perhaps along the adjacent creek. More formal analysis and dating of this feature and similar ones from the Montebello Islands is clearly warranted.

## 3.7 REE trends from Boodie Cave

The apparent trend of REE concentration with age was explored further with the dated samples from Boodie Cave (Table 3). As for the dunes, OSL ages show a positive correlation with the abundance of REE (and also of Zr), but there is a clear outlier in one sample (L008/15-8) from the lower units of excavation square E101/F101 at the front of Boodie Cave (Ward et al. 2017; their fig. 4). Sample L008/15-8 had the highest level of all REE elements and was given an OSL age of  $13.5 \pm 1.26$  ka,

based on central age modelling. However, when the finite mixture age estimate of  $38.1 \pm 4.3$  ka is used and plotted (Figure 10), a much better correspondence with REE is obtained and is also more consistent with the chronostratigraphy with an OSL age of  $47.2 \pm 4.7$  ka obtained from a sample ~ 10 cm below it (see Ward et al. 2017).

## 4.0 DISCUSSION

### 4.1 Changes in relative sea level

#### 4.1.2 *Changing island morphology and palaeoenvironmental context*

The analyses and observations from this study indicate that the dune deposits in the northernmost and southernmost parts of the island are mid- to late-Holocene in age, and overlie a reef platform of presumed last interglacial age. Around 80 ka, the morphology of Barrow Island was almost certainly smaller than it is today, with deposits above 6 m elevation (Figure 1) forming the main uplands within in a broad coastal plain (Figure 11).

In the Quarry area, laminated calcrete deposits over the reef base are dated to ~ 75 ka, based on both U-series dating and OSL dating of quartz within the calcrete. This was a period of increased moisture, at the end of the MIS-5 interstadial and beginning of MIS-4 stadial, as indicated from stalagmite records from Ledge Cave on Barrow Island (Conningham, 2017). Laminar calcrete can form at the base of dunes, through precipitation of calcite from carbonate-saturated water ponded above an impermeable layer (Semeniuk & Meagher, 1981; Arakel, 1982), which in this case would be last interglacial reef deposits. The NNW-SSE linear morphology of these calcrete deposits is consistent with this idea but would indicate crestlines perpendicular to the current coastal dunes, indicating a different formative wind direction, either from an extended period of changed wind directions and/or the influence of cyclones. Alternatively, they may reflect interdune areas subject to episodic flooding and evaporation. It is also possible that the linear features were originally deposited at the shoreline or in water, but there is insufficient information at present to investigate these ideas further.

On the NE tip of the island, at Surf Point (Figure 1), a chert manuport was found embedded into an old reef deposit – presumed to be of last interglacial age – near to calcrete that was dated by U-series to ~41 ka, and overlain by dune deposits dated by OSL to  $14.5 \pm 3.14$  ka (Ward et al., 2016). It is likely these calcrete deposits were similarly deposited in the water-saturated zone of former dune or interdune deposits that were later eroded to reveal the embedded manuport. Thus, whilst silicified limestone deposits on the island are not all the same age, they may represent wetter phases, although this is contradicted by the isotopic data from Boodie Cave that indicates increasing aridity around this time (Skippington et al., 2021). The coastline at this time would have been ~10 – 15 km away (Figure

11) and it is possible that calcrete formation is more linked in with vegetation and stabilisation of older dune systems.

For both the Quarry and Surf Point locations, the U-series and OSL ages bracket the known occupation of the island from 50 ka to 7 ka. The laminated calcrete deposits were clearly exploited for tool manufacture, although it is not known when it was exposed and accessible in amongst these dynamic sand bodies. There are no elements of the microlithic, bladelet, tula adze or hafted varieties of implements as documented from the larger western arid zone that might indicate earlier occupation during the mid- to late Holocene (Veth et al. in press).

At around 14 ka, relative sea level was rising very rapidly and passing through the range -70 to -50 m (Figure 3). Almost all the modern claypans on Barrow Island link to the coast through broad shallow ephemeral creeks, and artefact finds are concentrated with the claypan areas both in the island's north and south (Figure 2). At the drillpad claypan, clay sediments up to 60 cm deep are underlain by coarse gravel (used on the island as aggregate) that possibly indicates higher energy conditions and possibly higher freshwater runoff. Infilling of the claypans and the associated creeks is evident from the fining up sequence, albeit with some reworking of the sediments as implied from mixed OSL ages at 14 ka and 7 ka and the radiocarbon estimate for the *Terebralia* sp. at 11,359 – 11,876 cal BP (Wk-503029; Figure 7). Such reworking may result from processes of wetting and drying of the claypans and bioturbation by local fauna. A similar stratigraphic profile likely exists in the islands other claypans.

At present, significant rainfall results in ponding of water within these claypans and it is likely such areas formed a resource to past occupants. Such claypan contexts provide ecotones for a wide range of ethno-botanic resources; indeed, the highest diversity and richness of plants is recorded adjacent such drainage and 'wetland' areas in the Western Desert (Walsh & Veth, 1987). Combined with proximity to fuel timber and deeper sands for camping, lithic scatters are often spatially correlated to these features (Veth, 1993). The concentration of lithic artefacts on the claypan surfaces may also reflect a degree of localised reworking of artefacts in and around the claypans. However, in the absence of archaeological excavations of the claypans it remains uncertain whether any *in situ* cultural deposits exist at depth. Investigation would be warranted at the southern claypan scatters where erosional features show clay deposit depths of >10 cm.

To the southwest of Barrow Island, the modern 50 m bathymetric contour lies near the top of a relatively steep seabed slope, which means that at around 15 ka it would have formed a high-energy shoreline, not unlike today, and most likely to pass sediment along it to the NE and N. However, shallower contours, to around -15 m or so, are very different in shape, especially W and NW of the modern island. Thus, in general terms, inundation around the period 12–8 ka (the terminal Pleistocene) is likely to have seen a significant change in the coastline type, to one far more likely to have extensive intertidal areas and to form some productive coastal habitats for the island's

inhabitants, including intertidal flats, mangroves and coral reefs. This period may also have been a phase of increased dune formation because of an increased availability of fine sand at the coastline.

At 12 ka, RSL was ~40 m below present and nearing the end of a 2000-year long period of stillstand or slower rise (Figure 3). The shoreline was then ~10 km or so from the Boodie Cave archaeological site. The cave sediments reflect this, showing an increase in both the content of marine-derived sediments and culturally-derived marine fauna from this time (Ward et al., 2018). While not of the same volume or diversity as units dating to ~ 9 – 7 ka, there is an increase from four to over ten economic shellfish species in the cave deposits, with several baler shell knives and fragments, and an assemblage of *Dentalium* sp. beads dated to 12 ka (Veth et al., 2017).

By 10 ka, with RSL in the range -20 to -10 m (Figure 3 and 11), the coastline had probably advanced to within one or two kilometres of Boodie Cave, but was becoming steeper again, more exposed and less likely to retain sediments at the coast. The rate of rise in RSL began to slow, perhaps favouring the development of some useful coastal environments, but probably only locally in relatively sheltered areas such as on the northern side of Biggada Reef (Figure 1 and 2). The presence of mangroves on the western side of the island is indicated by various mangrove-associated midden and charcoal fragments in stratigraphic units of similar age in Boodie Cave (Veth et al., 2017) and by the ~ 11 ka *Terebralia* sp. shell in the drill-pad claypan in the southwest of the island.

The cluster of *Terebralia* sp. shells at Wapet Landing and on the Montebello Islands (where mangroves stands are also less extant) and immediately post-dating sea-level stabilisation, is also of interest as they demonstrate mangal deposits, albeit reworked, can survive in open contexts and maintain some spatial integrity. It is likely such deposits were more extensive in the past, and closer to their dates of deposition, and today only a small and residual sample survives. In Boodie Cave, the early Holocene units dating between ~ 9 – 7 ka are by far the richest archaeologically, with dense terrestrial faunal remains on which environmental studies are progressing (see Skippington et al., 2021) and also yielding significant quantities of marine fauna including fish, turtle, marine mammal, crab and sea urchin, and over 40 species of marine molluscs (Veth et al., 2017).

#### 4.1.2 *The Timing of Island Formation*

The above changes in RSL, combined with the associated environmental and sedimentary changes, indicate that Barrow Island and the adjacent Montebello Is. complex (Figure 11) have gone through several different physical and environmental configurations. Although there is uncertainty in the details, the general pattern is clear. At lowstand, the area was part of an extensive flat inland plain, at least 50 km across, with Barrow and Montebello Island forming isolated topographic highs behind an open arcuate coastline (Figure 11). With the Post-Glacial rise in RSL, the topographic highs were approached by the rising sea, first forming peninsulas (~15–10 ka) and later islands, including what is now Barrow Island and the various parts of the now Montebello Island complex. The precise timing

and details here are unknowable at present, primarily because there is no available information on the modern geological nature and past sedimentary evolution of the area that now forms the channel east of Barrow Island. At present, this channel contains a series of shallow sills at 10–14 m below LAT, and the shallowest at 6–6.5 m below LAT, i.e., ~ -8 m MSL, but it is unknown whether these are pre-Holocene features or modern mobile sediment – if the former, then it is possible that land connections persisted between Barrow Is. and the Montebello Islands within 2000 years or so before highstand.

There is similar uncertainty in the development of Mary Anne Passage, which now lies between the southern tip of Barrow Island and the mainland. This passage has its deepest point at around 10.5 to 11 m below LAT, i.e., ~12–12.5 m below MSL, and contains very large sand and gravel dunes (e.g., Lebec et al., 2021), interpreted as associated with flows generated during Tropical Cyclones (Larcombe et al., 2014), but the underlying geology is unknown and undated, as is the age of the basal unconsolidated sediments. Further, given the wide variety of past and present coastal processes along the Pilbara coastline, noted above, the precise timing of island formation - taken as the land being covered by seawater even at low water spring tides – thus remains unknown. Whilst it is perhaps most likely to be in the range of -11 to -8 ka, the geological and sedimentary uncertainties mean that it is perfectly possible to have been outside this range.

The sea-level index points present a continuous RSL rise during the early-to-mid Holocene (Figure 3). The record begins at 8.1 ka, where an index point places RSL at  $-6.4 \pm 0.2$  m. RSL rose to  $3.1 \pm 1.1$  m, indicating a sea-level highstand constrained by a marine limiting point at 6.0 ka. The late Holocene record is only constrained by a series of terrestrial limiting dates that shows RSL was below  $3.8 \pm 0.3$  m from 2.1 ka BP to present. Thus, overall, Post-Glacial RSL rose above existing levels before ~7 ka and may have gently fallen to present levels since then, although few data exist to constrain the mid- and late Holocene RSL.

Veth et al. (2017) interpreted the sediments of Boodie Cave to indicate its final stages of human occupation occurred in the period 7.2–6.8 ka (their fig. 3). This corresponds to a likely RSL at the time of -2 to +2 m, essentially the same as modern sea levels. Given the complexities of the area, including the ample availability of non-cohesive sediments, highly dynamic oceanographic processes - including waves, tidal currents and episodic cyclones - and the likely extensive shallow limestone-floored subtidal zones to the E and SW of the island, and that many of these factors are not yet constrained, it is impossible at present to determine whether the island had already been permanently cut off from the mainland. The abrupt end to cultural (but not sedimentary) deposits in Boodie Cave at ~ 7 ka does indicate some degree of island formation. Similarly, recent analyses of micro-fauna from Morgan's Cave on the Montebello islands and from owl pellet records on Barrow Island indicate a decline in species diversity consistent with island formation (Piper & Veth, 2021), with similar

patterns of diminished species diversity with decreased island size noted for other islands off Western Australia (Abbott & Wills, 2016).

Following the final stage of island formation, and its inferred abandonment by humans, all the open site contexts will have been subject to reworking, including by significant dune building in the Late Holocene and also more recently as indicated from the OSL chronology at the Quarry and Loop Beach. Dune stabilisation is favoured by vegetation cover but, much like today, vegetation cover was probably minimal beyond spinifex (*Triodia* sp.) and small stands of *Acacia* sp. and subject to frequent burning. The dune profile at Loop Beach, for example, shows around 50 cm of *net* sand accumulation over a burnt unit dated to 850–670 years ago (Figure 6) highlighting that fire and dune destabilisation was likely not infrequent. The emphasis here is on net sedimentation, because coastal dunes can grow in elevation by as much as 58–90 cm in a year or deflate by 60–75cm in a blowout over days or weeks (see Miyanishi & Johnson, 2021, and references therein). Recent observations (by PV and IW) of the removal of deposits by natural coastal processes from Hayne’s Cave, an early Holocene stratified midden site on the southern edge of the Campbell Island isthmus in the Montebello group, over a 30-year period indicates that even partially protected midden and artefacts can be significantly re-worked.

#### **4.2 Use of REE and grain micro-texture to inform sediment maturity**

Like much of the modern Pilbara coastline, Barrow Island is currently largely starved of terrigenous sediment, so that the sediments available for accumulation largely derive from locally reworked material from coastal and inner-shelf sources. For much of the last 80 ka and including the initial period of occupation at ~ 50 ka, coastal plain sediments will have included reworked weathered material from the granitic and metasedimentary hinterland to the south, the distant coast to the north, and more locally of weathered material from local limestone bedrock to form *terra rossa* soils (Ward et al., 2017; 2018). The low rates of clastic sediment supply, long periods of weathering and abrasion, combined with high energy wave and changing sea levels (especially marine transgressions) will have promoted the preferential accumulation of heavy mineral sands from the shelf onto the past and present coast (Roy, 1999; Jaireth et al., 2014). Intense weathering will also have promoted concentration of resistant minerals, especially quartz, and heavy minerals, especially within remnant dune and palaeosol deposits or trapped deep within caves (Ward et al., 2018).

A relationship with sediment weathering and compositional maturity is indicated from the positive correlation of REE with age in dated sediments from both the cave and dunes, albeit with an outlier with the young age estimates for red dune deposits at the Chair (BIC19-1) (Figure 10). Even for Fonz’ gravel pit, the older estimate of  $14.4 \pm 0.97$  ka (Shfd20006) in the mixed age modelling is more consistent with the high REE abundances. Intense weathering is also reflected in high ratios of Th/U (> 5), mainly as high Th values (> 10 ppm) and including locations as diverse as the claypan

sediments from the gravel pit site, the red sediments at Loop beach, the quartz-rich red dune, and also sediments within Boodie Cave that are older than ~ 38 ka (this includes the modified age estimate for L008/15-8). Hence in coastal sediments from this region, it may be possible that some general indication of relative age may be provided by the REE abundance.

However, the question arises as to whether heavy minerals are the only source of REE. For example, REE-bearing phosphate minerals, such as monazite or xenotime, may also be potential contributing phases. Secondary phosphate minerals in caves can form from guano-derived leachates or bone deposits (Karkanis et al., 2002), with a Croatian cave study finding an association of REE with bat guano and a slight enrichment of LREE and depletion of HREE (Miko et al., 2002). Whilst there are colonies of microbats in Boodie Cave, mineral analyses indicate that the major contributor of phosphate is bone apatite with only trace (< 0.1%) quantities of the phosphate minerals monazite and xenotime (Ward et al., 2018). However, there is a consistent enrichment of LREE over HREE in the Boodie Cave sediments that does indicate leaching, hence further investigation of the relative contributions of primary and secondary minerals to REE abundance is needed.

#### *4.2.3 Caution in the use of colour as a guide to age*

With the early Holocene approach of the shoreline near Boodie Cave, and likely switching on of some coastal coral reefs, any mature mineral-rich sands will have been increasingly mixed with fresh, biogenic carbonate material, as evident from the clear decline in heavy minerals (and REE) within the Boodie Cave sediments (Ward et al., 2018). Even once the mid-Holocene sea-level had stabilised, reworking and pedogenic weathering of mature red sediments will have continued and become mixed to varying extents with fresh biogenic carbonates. With increasing pedogenesis, acidity increases, so that carbonate is leached and may be reprecipitated at depth.

Mixing and pedogenesis are also reflected in the high content of carbonate (>85%), and low aluminosilicate (Al, Ti, K) and oxide (Fe-Mn) within the contemporary nearshore dunes, and the low content of carbonate (<50%), aluminosilicate and oxide in the dune and claypan deposits inland of the present coast. Over time, ongoing pedogenesis may subsequently leach out iron oxides to leave bleached quartz (Turner et al., 2018). Hence it is possible that the quartz-rich dunes in the north of the island reflect such long-term pedogenesis because the red colouration is readily removed from the quartz grains through acidification (Figure 9) perhaps reflecting more recent rubefaction. Rubefaction reflects the intensity as much as the duration of pedogenesis, with the timespan necessary to obtain a homogenous red coating in the order of a few hundred to a few thousand years depending on the environment (Schwertmann, 1992). Pure quartz sands have also been recorded (by IW) on the Lowendal Islands approximately 6 km NE of Barrow Island (Figure 1), with further work ongoing to explore the distribution of these quartz-rich deposits within the limestone-based Barrow-Montebello Island complex.

Interpretations based on hue of sediments may only be useful where there is a common burial history and this is difficult to demonstrate for non-cohesive sediments in such a physically dynamic and evolving environment. Across the island, the colour of the dune sands varies considerably with location and depth in the profile, as the concentration of carbonate and iron oxide minerals changes. These changes in colour may also result from variations in other factors such as water regimes, which accelerate weathering and leaching (Turner et al., 2018) and organic content, including burnt plant fragments, that may affect pH (e.g., Pitts & Clarke, 2020). Leaching may also account for the high Th/U ratios, and enrichment of LREE over HREE in the chronologically older and for the cave sediments, more deeply buried, sediments (Figure 10).

A key implication is that the colour as seen today cannot be used as a reliable guide to the age of accumulation, nor as an indicator of the potential age of any contained archaeological material. Lessa & Masselink (2006) observed similar uncertainty for the sediment deposits behind Cable Beach, Broome, that had previously been considered to comprise white Holocene-age coastal dune and beach deposits and inland, Pleistocene-age pink or brown sediments. However, a beachrock deposit that was overlain by reddish and then white sands was dated to  $3180 \pm 90$  14C yrs BP (SUA-1722), indicating that the whole barrier was Holocene (Lessa & Masselink, 2006). Yet, even this observation only reflects the most recent formation history of the barrier system and cannot exclude the possibility of an older, sedimentologically-mature origin for pink or brown sediments. Assumed terminal Pleistocene-aged red dunes in the west Kimberley were also shown to be much younger, containing late Holocene middens which had slumped giving them a deeply stratified appearance (O'Connor & Veth, 1993).

#### *4.2.4 Grain micro-texture as an indicator of palaeoenvironment and weathering*

As outlined above, coastal dune systems are the net result of erosion, transport and deposition of sand by both wind and waves and unless they are indurated or deeply buried, they retain the potential along with cultural material associated with them, to be eroded and reworked many times over particularly during cyclones and by persistent seasonal winds. Whilst OSL dating can only provide an indication of the most recent phase of dune accumulation, some insight into the history of the dunes may also be gained from a morphological and microtextural analysis of their quartz grains (Krinsley & Smalley, 1972; Vos et al., 2014).

As may be expected polygenic micro-textures dominate most samples, indicating significant overprinting by remobilisation and some mixing of grains of different origin within the coastal dunes. For example, v-shaped percussion cracks inherited from previous sedimentary cycles may be observed on quartz grains from littoral dunes and low-energetic, sub-aqueous environments (Vos et al., 2014). The sampled white/pink dunes (e.g., BIQ19-1 and BIC19-4) comprise angular, pitted grains with straight and v-shaped grooves resulting from grain-to-grain collision in high energetic

sub-aqueous environments mixed with grains with bulbous edges and abundant crescentic marks that have been enhanced (widened) through chemical weathering. It is likely the high-energy intertidal environment has been the main source of grains to foredune sedimentary system, and this has included recycled aeolian sediments that have become mixed with sediments in the littoral zone.

In contrast, the older, red dune sands tend to show sub-rounded to rounded outline, upturned plates, (remnant) crescentic percussion marks, and occasional meandering ridges and abrasion fatigue (and no v-shaped pits), which indicate that aeolian transport was more dominant (Vos et al., 2014).

Pedogenic alteration of quartz grains, manifest as solution and reprecipitation features, has likely destroyed many of the original mechanical textures within these dune sediments. For the quartz-rich red dune, grains microtextures also include features diagnostic of aeolian transport, including rounded to sub-rounded, med-high sphericity, crescentic marks, meandering ridges, bulbous edges, and occasional chattermarks. According to Peterknechet and Tietz (2011), the latter form by blunt collisions during transport but only become visible through dissolution during a depositional stage in a tropical/sub-tropical climate. Further evidence of the latter includes both triangular and occasional rhomboidal solution pits. It is possible this dune represents an isolated dune from an old storm deposit that has been intensely weathered and leached over time.

Studies are ongoing to further explore the textural features of quartz grains from both the archaeological sites and from the modern island contexts to better understand sediment provenance and reworking, and will be the subject of a separate paper.

## **5.0 CONCLUSION**

This study has undertaken some preliminary dating and characterisation of sediments from ‘offsite’ contexts around Barrow Island. Both geology and sedimentology underpin cultural inferences and interpretations of chronology. The results provide initial evidence for the pre-occupation (> 50 ka) Barrow Island morphology essentially defined by deposits above the 6 m contour in what would have been an expansive coastal plain. Now eroded dune systems formed over probable last interglacial reef deposits in the north of the island and promoted the formation of calcrete deposits dated to ~ 80 ka at the Quarry that were later exploited for tool manufacture, and also around 41 ka that embedded an artefact at Surf Point.

New sea-level modelling has helped constrain changing oceanographic and sedimentary processes for the area, especially when past sea levels were within 25 m of modern levels. We infer a transition around 15 ka from a high-energy shoreline to a more tide-dominated shoreline at the terminal Pleistocene (12-8 ka) with extensive intertidal areas and dune-building along the littoral, consistent with greater and more diverse coastal and marine cultural assemblages in Boodie Cave. Residual

*Terebralia* sp. shell deposits from this period and immediately post-dating the Holocene sea-level stabilisation help indicate that past mangrove systems were much larger than those of today. Whilst the complex geology, bathymetry and sediment dynamics of the Barrow Is. region mean that the precise timing of island formation cannot be determined, the cultural record indicates diminished species diversity and cessation of occupation after 7.2-6.8 ka.

Although only eleven OSL ages are reported, they clearly indicate that sediment colour is not a good indicator of depositional age, probably because coastal sediments are continually reworked. This reworking is clear from the multiple overprinting of micro-textures on quartz grains from the dune sands, and in the case of the quartz-rich sediments, multiple cycles of leaching and rubefaction. Nor is numeric age a good guide to sediment compositional and textural maturity, as many dunes are polygenic and contain grains that have undergone many cycles of reworking. A positive correlation of REE abundances with absolute age provides some indication of heavy mineral abundance and by association, sediment maturity, and potentially offers a means of testing chronological uncertainties. Accordingly, the maturity and depositional history of these sediments may need to be better understood in order to assign any relative age to associated cultural materials.

### **Author contributions**

IW and PL were responsible for the Conceptualization of the overarching research aims and objectives, with field sampling undertaken by IW and MB. IW was responsible for the design of Methodology, with formal analysis undertaken by MB (OSL dating), Pete Scott (U-series dating), TL, KM, NK, PL (sea-level modelling and text), IW (sediment analysis). IW is responsible for writing the initial draft with all authors responsible for writing, review & editing the revised manuscript. IW, MB and TL were responsible for the production of figures. We thank Colin Murray-Wallace and one other anonymous reviewer for their helpful comments.

### **Data availability**

Data available on request from the authors.

### **Declaration of competing interest**

The authors declare that they have no known competing financial interests or personal relationships that could have appeared to influence the work reported in this paper.

### **Acknowledgements**

This study was made possible through a Research Collaboration Award from the University of Western Australia, with additional funding provided from an Australian Research Council Discovery Early Career Award to IW (DE180100601). Archaeological data was collected by the Barrow Island Archaeological Project funded by an ARC Discovery Grant (DP130100802) 2013–2015 awarded to PV and team. Department of Biodiversity Conservation and Attractions, Chevron Australia and WA

Oil are thanked for their logistical and personnel support in the field, as also are Mick O’Leary and Peter Kendrick. We acknowledge the support of Buurabalayji Thalanyji Aboriginal Corporation.

We thank Dick Peltier for providing the ICE-7G\_NA ice model and Kurt Lambeck and Anthony Purcell for providing the ANU-ICE ice model. The global ANU-ICE combination model used in this study was kindly provided by Holger Steffen. Tanghua Li is supported by the Singapore Ministry of Education Academic Research Fund MOE2019-T3-1-004 and MOE2018-T2-1-003, the National Research Foundation Singapore, and the Singapore Ministry of Education, under the Research Centers of Excellence initiative. The GIA modelling is conducted in part using the research computing facilities and/or advisory services offered by Information Technology Services, the University of Hong Kong. This work comprises Earth Observatory of Singapore contribution no. 424.

The authors also acknowledge the facilities, and the scientific and technical assistance of Microscopy Australia at the Centre for Microscopy, Characterisation & Analysis, the University of Western Australia, a facility funded by the University, State and Commonwealth Governments.

Acknowledgement is given to Mark Basgall David Zeanah and David Glover of Sacramento University for use of artefact distribution maps; and to Mick O’Leary for the DEM image of the Chair (Loop Beach).

## REFERENCES

- Abbott, I., Wills, A., 2016. *Review and synthesis of knowledge of insular ecology, with emphasis on the islands of Western Australia*. Conservation Science Western Australia, Volume 11. 206pp.
- Arakel, A.V., 1982. Genesis of calcrete in Quaternary soil profiles, Hutt and Leeman Lagoons, Western Australia. *J. Sedimentary Petrology*, **52**, 109–125.
- Baker, R.G.V., Haworth, R.J., Flood, P.G., 2005. An oscillating Holocene sea-level? Revisiting Rottnest Island, Western Australia, and the Fairbridge eustatic hypothesis. *Journal of Coastal Research, Special Issue* **42**, 3-14.
- Bateman M.D., Catt, J.A., 1996. An absolute chronology for the raised beach and associated deposits at Sewerby, East Yorkshire, England. *J. Quaternary Science*, **11**(5), 389–395.
- Bateman, M.D., Frederick, C.D., Jaiswal, M.K., Singhvi, A.K., 2003. Investigations into the potential effects of pedoturbation on luminescence dating. *Quaternary Science Reviews*, **22** (10-13), 1169–1176.
- Bateman, M.D., Boulter, C.H., Carr, A.S., Frederick, C.D., Peter, D., Wilder, M., 2007. Detecting post-depositional sediment disturbance in sandy deposits using optical luminescence. *Quaternary Geochronology*, **2** (1–4), 57–64
- Benjamin, J., O’Leary, M., McDonald, J., Wiseman, C., McCarthy, J., Beckett, E., Morrison, P., Stankiewicz, F., Leach, J., Hacker, J., Baggaley, P., Jerbić, K., Fowler, M., Fairweather, J., Jeffries, P., Ulm, S., Bailey, G., 2020. Aboriginal artefacts on the continental shelf reveal ancient drowned cultural landscapes in northwest Australia. *Plos One*, **15**(7), e0233912.
- Byrne, C., Dooley, T., Manne, T., Paterson, A., Dotte-Sarout, E., 2020. Island survival: The anthracological and archaeofaunal evidence for colonial-era events on Barrow Island, north-west Australia. *Archaeology in Oceania* **55** (1), 15–32.
- Carrigy, M.A., Fairbridge, R.W., 1954. Recent sedimentation, Physiography and structure of the continental shelves of Western Australia. *Journal of the Royal Society of Western Australia* **38**, 65-95

Chevron Australia, 2005. Draft Gorgon Environmental Impact Statement/Environmental Review and Management Programme for the Proposed Gorgon Development. Chevron Australia, Perth, Western Australia.

Collins, L.B., Zhao, J., Freeman, H., 2006. A high-precision record of mid-late Holocene sea-level events from emergent coral pavements in the Houtman Abrolhos Islands, southwest Australia. *Quaternary International* **145**, 78-85.

Condie, S., Andrewartha, J., Mansbridge, J., Waring, J., 2006. Modelling circulation and connectivity on Australia's North West Shelf. NWSJEMS Technical Report No. 6. Available at [https://www.cmar.csiro.au/nwsjems/reports/NWSJEMS\\_final.pdf](https://www.cmar.csiro.au/nwsjems/reports/NWSJEMS_final.pdf)  
Accessed 1 July 2021.

Conningham, K. 2017. A 130 to 61 ka climate reconstruction from Barrow Island, north-western Australia. Unpublished Honours thesis, James Cook University.

Denniston, R., Asmerom, Y., Lachniet, M., Polyak, V., Hope, P., An, N., Rodzinyak, K. and Humphreys, W., 2013. A Last Glacial Maximum through middle Holocene stalagmite record of coastal Western Australia climate. *Quaternary Science Reviews*, **77**, 101–112.

Ditchfield, K. 2018. Pleistocene – Holocene Coastal Mobility Patterns in the Carnarvon Bioregion, Northwestern Australia. Unpublished PhD thesis. The University of Western Australia.

Ditchfield, K., Manne, T., Hook, F., Ward, I., Veth, P., 2018. Coastal occupation before the Big Swamp: Results from excavations at John Wayne Country rock shelter on Barrow Island. *Archaeology in Oceania*, **53** (3), 163–178.

Ditchfield, K., Ward, I. 2019. Local lithic landscapes and local source complexity: Developing a new database for geological sourcing of archaeological stone artefacts in North-Western Australia. *J. Archaeological Science: Reports*, **24**, 539–555.

Dominey-Howes D., 2007. Geological and historical records of tsunami in Australia. *Marine Geology*, **239**, 99–123

Dufois F, Lowe RJ, Branson P, Fearn P., 2017. Tropical cyclone-driven sediment dynamics over the Australian North West Shelf. *Journal of Geophysical Research: Oceans* **122**, 225-244.

Duller, G. A. T., 2003. Distinguishing quartz and feldspar in single grain luminescence measurements. *Radiation Measurements* **37**, 161-165.

Eisenhauer, A., Wasserburg, G.J., Chen, J.H., Bonani, G., Collins, L.B., Zhu, Z.R., Wyrwoll, K.H., 1993. Holocene sea-level determination relative to the Australian continent: U/Th (TIMS) and <sup>14</sup>C (AMS) dating of coral cores from the Abrolhos Islands. *Earth and Planetary Science Letters* **114**, 529-547.

Engelhart, S., Peltier, W.R., Horton, B.P., 2011, Holocene relative sea-level changes and glacial isostatic adjustment of the US Atlantic coast. *Geology*, **39**, 751-754

Fairbridge, R.W., 1960. The changing level of the sea. *Scientific American* **202**, 70–79.

Fairbridge, R.W., 1961. Eustatic changes in sea level. *Physics and Chemistry of the Earth* **4**, 99–185.

Guerin, G., Mercier, N., Adamic, G., 2011. Dose-rate conversion factors: update. *Ancient TL* **29**, 5–8.

Heaton, T.J., Köhler, P., Butzin, M., Bard, E., Reimer, R.W., Austin, W.E.N., Bronk Ramsey, C., Grootes, P.M., Hughen, K.A., Kromer, B., Reimer, P.J., Adkins, J., Burke, A., Cook, M.S., Olsen, J.,

Skinner, L.C., 2020. Marine20—The Marine Radiocarbon Age Calibration Curve (0–55,000 cal BP). *Radiocarbon*, **62**(4), 779–820.

Hickman, A.H., Strong, C.A., 2003. Dampier – Barrow Island Western Australia. Geological Survey of Western Australia 1:250 000 Geological Series — Explanatory Notes (2<sup>nd</sup> Ed). Available at available via <http://www.dmp.wa.gov.au>

Hijma, M.P., Engelhart, S.E., Törnqvist, T.E., Horton, B.P., Hu, P., Hill, D.F., 2015, A protocol for a geological sea-level database. Pp. 536-553. In: Shennan, I., Long, A.J., Horton, B.P. (ed.) *Handbook of Sea-Level Research*, Wiley Blackwell.

Hook, F., McDonald, J., Paterson, A, Souter, C., Veitch, B., 2004, Cultural Heritage Assessment and Management Plan—Proposed Gorgon Development, Pilbara, North Western Australia April 2004. In: Draft Environmental Impact Statement/Environmental Review and Management Programme for the Proposed Gorgon Development. Technical Appendix E1. Gorgon Australian Gas.

Jaireth, S., Hoatson, D. M., Mieuzitis, Y., 2014. Geological setting and resources of the major rare-earth-element deposits in Australia. *Ore Geology Reviews*, **62**, 72–128

James, N.P., Bone, Y., Kyser, T.K., Dix, G.R., Collins, L.B., 2004. The importance of changing oceanography in controlling late Quaternary carbonate sedimentation on a high energy, tropical oceanic ramp: north-western Australia. *Sedimentology* **51**, 1179-1938.

Karkanas, P. & Goldberg, P., 2019. Reconstructing archaeological sites. Understanding the Geoarchaeological Matrix. John Wiley & Sons, West Sussex.

Karkanas P., Rigaud J.P., Simek J.F., Albert R.M., Weiner S., 2002 Ash bones and guano: a study of the minerals and phytoliths in the sediments of Grotte XVI, Dordogne, France. *Journal of Archaeological Science*, **29** (7), 721-732.

Kendrick, P.G., Mau, R. 2003. Carnarvon 1 (CAR 1 Cape Range Subregion). In: May, J.E., McKenzie, N.L. (Eds.) *A biodiversity audit of Western Australia's 53 biogeographical subregions in 2002. Report for the national land and water resources audit biodiversity assessment*. Department of Conservation and Land Management, Perth, Western Australia.

Khan, N.S., Horton, B.P., Engelhart, S., Rovere, A., Vacchi, M., Ashe, E.L., Törnqvist, T.E., Dutton, A., Hijma, M.P., Shennan, I., 2019. Inception of a global atlas of sea levels since the Last Glacial Maximum. *Quaternary Science Reviews*, **220**, 359-371.

Krinsley, D.H., Smalley, I.J., 1972. The study of quartz sand in sediments provides much information about ancient geological environments. *America Scientist*, **60**(3), 286–291.

Lambeck, K., 2002. Sea level change from Mid Holocene to Recent time: An Australian example with global implications. In: Mitrovica, J.X., Vermeersen, B. (Eds.), *Ice Sheets, Sea Level and the Dynamic Earth*, **29**, 33-50.

Lambeck, K., Purcell, A., 2005. Sea-level change in the Mediterranean Sea since the LGM: model predictions for tectonically stable areas. *Quaternary Science Reviews*, **24**(18-19), 1969–1988.

Lambeck, K., Rouby, H., Purcell, A., Sun, Y., Sambridge, M., 2014. Sea level and global ice volumes from the Last Glacial Maximum to the Holocene. *Proc. National Academy of Sciences*, **111**(43), 15296–15303.

- Lambeck, K., Purcell, A., Zhao, S., 2017. The North American Late Wisconsin ice sheet and mantle viscosity from glacial rebound analyses. *Quaternary Science Reviews*, **158**, 172–210.
- Larcombe, P., Woolfe, K.J., 1999. Terrigenous sediments as influences upon Holocene nearshore coral reefs, central Great Barrier Reef, Australia. *Australian Journal of Earth Sciences*, **46**, 141-154.
- Larcombe, P., Huang, P., Pusey, G., 2014. From marine geomorphology to turbulence: Some implications of sediment transport for developments on the NW Australian continental margin. Perth: Australian Oil & Gas (AOG).
- Larcombe, P., Ward, I. A. K., Whitley, T., 2018. Physical sedimentary controls on subtropical coastal and shelf sedimentary systems: Initial application in conceptual models and computer visualizations to support archaeology. *Geoarchaeology*, **33**, 6, 661–679
- Lebecq, U., Paumard, V., O’Leary, M.J., Lang, S., 2021. Towards a regional high-resolution bathymetry of the North West Shelf of Australia based on Sentinel-2 satellite images, 3D seismic surveys and historical datasets. *Earth Systems Science Data*, **13**, 5191–5212.
- Lessa, G., Masselink, G., 2006. Evidence of a mid-Holocene sea level highstand from the sedimentary record of a macrotidal barrier and palaeoestuary system in Northwestern Australia. *J. Coastal Research*, **22**(1), 100–112.
- Lewis, S.E., Sloss, C.R., Murray-Wallace, C.V., Woodroffe, C.D., Smithers, S.G., 2013. Post-glacial sea-level changes around the Australian margin: a review. *Quaternary Science Reviews*, **74**, pp.115-138.
- Li, T., Wu, P., Steffen, H., Wang, H., 2018. In search of laterally heterogeneous viscosity models of glacial isostatic adjustment with the ICE-6G\_C global ice history model. *Geophysical Journal International*, **214**(2), 1191–1205.
- Li, T., Wu, P., 2019. Laterally heterogeneous lithosphere, asthenosphere and sub-lithospheric properties under Laurentia and Fennoscandia from Glacial Isostatic Adjustment. *Geophysical Journal International*, **216**(3), 1633–1647.
- Linse, A.R., 1993. Geoarchaeological scale and archaeological interpretation: Examples from the central Jornada Mogollon. *Geological Society of America Special Paper* **283**, 11-28.
- Lynch, J.A., Beeton, R.J.S., Greenslade, P., 2019. The conservation significance of the biota of Barrow Island, Western Australia. *J. Royal Society of Western Australia*, **102**, 98–133
- Lynn, W.C., Pearson, M.J., 2000. The Color of Soil. *The Science Teacher* **67** (5), 20–23.
- McNamara, K.J., Kendrick, G.W. 1994., Cenozoic Molluscs and Echinoids of Barrow Island, Western Australia. *Records of the Western Australian Museum, Perth, Western Australia*. Supplement **51**, 1–50.
- May, S.M., Brill, D., Engel, M., Scheffers, A., Pint, A., Opitz, S., Wennrich, V., Squire, P., Kelletat, D., Brückner, H., 2015, Traces of historical tropical cyclones and tsunamis in the Ashburton Delta (northwest Australia). *Sedimentology*, **62**, 1546-1572.
- May, S.M., Falvard, S., Norpoth, M., Pint, A., Brill, D., Engel, M., Scheffers, A., Dierick, M., Paris, R., Squire, P., 2016, A mid-Holocene candidate tsunami deposit from the NW Cape (Western Australia). *Sedimentary Geology*, **332**, 40-50.
- May, S.M., Gelhausen, H., Brill, D., Callow, J.N., Engel, M., Opitz, S., Scheffers, A., Joannes-Boyau, R., Leopold, M., Brückner, H., 2018, Chenier-type ridges in Giralia Bay (Exmouth gulf, Western

- Australia)-processes, chronostratigraphy, and significance for recording past tropical cyclones. *Marine Geology*, **396**, 186-204.
- McDonald, J., Reynen, W., Blunt, Z., Ditchfield, K., Leopold, M., Monks, C., Dortch, J., Veth P., 2022. Enderby Island Excavations Area 2. In: McDonald, J., Mulvaney, K., Paterson, A., Veth, P. (Eds.). *Murujuga: Dynamics of the Dreaming. Rock art, stone features and excavations across the Dampier Archipelago*. CRAR+M Monograph No. 2. Perth, UWA Press.
- Moro, D., Lagdon, R., 2013. History and environment of Barrow Island. *Records of the Western Australian Museum*, **83**, 1–8 (Suppl.).
- Miko, S., Kuhta, M., Kapelj, S., 2002. Environmental baseline geochemistry of sediments and percolating waters in the Modrič Cave, Croatia. *Acta Carsologica* **31**(1) 135-149.
- Miyanishi, K., Johnson, E.A. 2021. Coastal dune succession and the reality of dune processes. In: Johnson, E.A., Miyanishi, K. (Eds.) *Plant Disturbance Ecology*. Academic Press, pp. 253-290.
- Murray, A.S., Wintle, A.G., 2000. Luminescence dating of quartz using an improved single-aliquot regenerative-dose protocol. *Radiation Measurements* **32**, 57–73.
- Murray A.S., Wintle, A.G., 2003. The single aliquot regenerative dose protocol: potential for improvements in reliability. *Radiation Measurements* **37**, 377–381.
- Nakada, M., Lambeck, K., 1989. Late Pleistocene and Holocene sea-level change in the Australia region and mantle rheology. *Geophysical Journal* **96**, 497-517.
- O'Connor, S., Veth, P., 1993. Where the desert meets the sea: a preliminary report of the archaeology of the southern Kimberley coast. *Australian Archaeology* **37**, 25-34.
- O'Leary, M., Paumard, V., Ward, I., 2020. Exploring Sea Country through high-resolution 3D seismic imaging of Australia's NW shelf. *Quaternary Science Reviews* **239**,  
<https://doi.org/10.1016/j.quascirev.2020.106353>
- Paterson, A., 2017. Unearthing Barrow Island's Past: The Historical Archaeology of Colonial-Era Exploitation, Northwest Australia. *Int. Journal of Historical Archaeology* **21**, 346–368.
- Paterson, A., Veth, P., 2020. The point of pearling: Colonial pearl fisheries and the historical translocation of Aboriginal and Asian workers in Australia's Northwest. *J. Anthropological Archaeology*, **57**, 101143.
- Pearce, A., Buchan, S., Chiffings, T., D'Adamo, N., Fandry, C., Fearn, P.R.C.S., Mills, D. J., Phillips, R. C., Simpson, C., 2003. A review of the oceanography of the Dampier Archipelago, Western Australia. In: Wells, F.E., Walker, D.I., Jones, D.S., editors. *The Marine Flora and Fauna of Dampier, Western Australia*. Perth: Western Australian Museum; pp. 13-50.
- Peltier, W. R., Argus, D. F., Drummond, R., 2015. Space geodesy constrains ice age terminal deglaciation: The global ICE-6G\_C (VM5a) model. *JGR Solid Earth*, **120** (1), 450-487.
- Peterknecht, K.M., Tietz, G. F., 2011. Chattermark Trails: Surface Features on Detrital Quartz Grains Indicative of A Tropical Climate. *Journal of Sedimentary Research*, **81**, 153–158.
- Piper, C. J., Veth, P.M., 2021. Palaeoecology and sea level changes: Decline of mammal species richness during late Quaternary island formation in the Montebello Islands, north-western Australia. *Palaeontologia Electronica*, **24**(2), a20. <https://doi.org/10.26879/1050>

- Pitts, K.M., Clarke, R.M., 2020. The forensic discrimination of quartz sands from the Swan Coastal Plain, Western Australia. *Forensic Science International: Reports*, **2**, 100130
- Playford, P.E., 2014. Recent mega-tsunamis in the Shark Bay, Pilbara, and Kimberley areas of Western Australia. *J. Royal Society of Western Australia*, **97**, 173–188.
- Playford, P.E., Cockbain, A.E., Berry, P.F., Roberts, A.P., Haines, P.W., Brooke, B.P., 2013. *The geology of Shark Bay*. Geological Survey of Western Australia, Bulletin 146, 281p.
- Prescott, J.R., Hutton, J.T., 1994. Cosmic-Ray Contributions to Dose-Rates for Luminescence and ESR Dating - Large Depths and Long-Term Time Variations. *Radiation Measurements* **23**, 497–500.
- Ramos-Vázquez, M.A., Armstrong-Altrin, J.S., 2020. Provenance and palaeoenvironmental significance of microtextures in quartz and zircon grains from the Paseo del Mar and Bosque beaches, Gulf of Mexico. *J. Earth Sys. Sci.*, **129** (1), 1-16.
- Roy, P.S., 1999. Heavy mineral beach placers in southeastern Australia; their nature and genesis. *Economic Geology* **94** (4), 567–588.
- Roy, K., Peltier, W. R., 2017. Space-geodetic and water level gauge constraints on continental uplift and tilting over North America: regional convergence of the ICE-6G\_C (VM5a/VM6) models. *Geophysical Journal International*, **210**(2), 1115–1142.
- Roy, K., Peltier, W. R., 2018. Relative sea level in the Western Mediterranean basin: A regional test of the ICE-6G\_NA (VM7) model and a constraint on late Holocene Antarctic deglaciation. *Quaternary Science Reviews*, **183**, 76–87.
- Scheffers, S.R., Scheffers, A., Kelletat, D., Bryant, E.A., 2008. The Holocene paleo-tsunami history of West Australia, *Earth and Planetary Science Letters*, **270**, 137-146.
- Schwertmann, U., 1992. Relations between iron oxides, soil colour, and soil formation. *Soil Science Society of America, Special Publication*, **31**, 51-69.
- Scott, P.M. 2019. Geochemical records in travertine veins at the Green River CO<sub>2</sub> seeps (Utah); Doctoral Thesis; University of Cambridge.
- Searle, D.J., Woods, P.J., 1986. Detailed documentation of a Holocene sea-level record in the Perth region, southern Western Australia. *Quaternary Research*, **26**, 299-308
- Shennan, I., Horton, B., 2002, Holocene land and sea-level changes in Great Britain. *Journal of Quaternary Science: Published for the Quaternary Research Association*, **17**, 511-526.
- Shennan, I., Long, A.J., Horton, B.P., 2015, *Handbook of sea-level research*. John Wiley & Sons
- Semeniuk V. Meagher, T.D., 1981. Calcrete in Quaternary coastal dunes in south western Australia: a capillary-rise phenomenon associated with plants. *J. Sedimentary Petrology*, **51**, 47–68.
- Skippington, J., Manne, T., Veth, P., 2021. Isotopic indications of Late Pleistocene and Holocene paleoenvironmental changes at Boodie Cave Archaeological Site, Barrow Island, Western Australia. *Molecules* **26**, 2582. <https://doi.org/10.3390/molecules26092582>
- Smith, J.A., Wright, L.J., Morris, K.D., 2006. BiblioBarrowIsland – An Annotated Bibliography of the Natural History of Barrow Island 1622 – 2004. *Conservation Science Western Australia*, **5**(3), 296–364.

- Souter, C., Paterson, A., Hook, F., 2006. The assessment of archaeological sites on Barrow Island and the Dampier Archipelago, Pilbara, Western Australia: a collaborative approach. *Bulletin of the Australasian Institute for Maritime Archaeology*, **30**, 86–94
- Spooner, P.T., Chen, T., Robinson, L.F., Coath, C.D., 2016. Rapid uranium-series age screening of carbonates by laser ablation mass spectrometry, *Quaternary Geochronology* **31**, 28–39
- Turner, B.L., Hayes, P.E., Laliberté, E. 2018. A climosequence of chronosequences in southwestern Australia. *European Journal of Soil Science* **69**, 69–85.
- Twiggs, E.J., Collins, L.B., 2010, Development and demise of a fringing coral reef during Holocene environmental change, eastern Ningaloo Reef, Western Australia. *Marine Geology*, **275**, 20–36.
- van de Plassche, O., van der Borg, K., de Jong, A.F., 1998, Sea level–climate correlation during the past 1400 yr. *Geology*, **26**, 319–322.
- Veth, P.M. 1993 Islands in the Interior: The Dynamics of Prehistoric Adaptations within the Arid Zone of Australia. *International Monographs in Prehistory. Archaeological Series 3*. Ann Arbor, Michigan.
- Veth, P., Ditchfield, K., Hook, F., 2014. Maritime deserts of the Australian northwest. *Australian Archaeology*, **79**(1), 156–166.
- Veth, P., McDonald, J. and P. Hiscock in press Beyond the Barriers: a new model for the settlement of Australian Deserts. In McNiven, I. and B. David (eds,) *Reader for Australian Archaeology*. Oxford University Press, Oxford.
- Veth, P., Aplin, K., Wallis, L., Manne, T., Pulsford, T., White, E., Chappell, A., 2007. *The Archaeology of Montebello Islands, North-West Australia: Late Quaternary foragers on an arid coastline*. Archaeopress.
- Veth, P., Ward, I., Manne, T., Ulm, S., Ditchfield, K., Dortch, J., Hook, F., Petchey, F., Hogg, A., Questiaux, D., Demuro, M., Arnold, L., Spooner, N., Levchenko, V., Skippington, J., Byrne, C., Basgall, M., Zeanah, D., Belton, D., Helmholtz, P., Bajkan, S., Bailey, R., Placzek, C., Kendrick, P. 2017. Early human occupation of a maritime desert, Barrow Island, North-West Australia. *Quaternary Science Reviews*, **168**, 19–29.
- Vos, K., Vandenberg, N., Elsen, J., 2014. Surface textural analysis of quartz grains by scanning electron microscopy (SEM): From sample preparation to environmental interpretation. *Earth Science Reviews*, **128**, 93–104.
- Walsh, F., Veth, P., 1987. The influence of the spatial and temporal distribution of plant food resources on traditional Martujarra subsistence strategies. *Australian Archaeology*, **25**, 88–101.
- Ward, I., Veth, P., Manne, T., 2014. To the islands born: the research potential of submerged landscapes and human habitation sites from the islands of NW Australia. In: Harff, J., Bailey, G. & Luth, F. (Eds.) *Geology and Archaeology: Submerged Landscapes of the Continental Shelf*. Geological Society, London, Special Publications, **411**, 251–263.
- Ward, I., Salvemini, F., Veth, P., 2016. 3D visualisation and dating of an embedded chert artefact from Barrow Island. *J. Archaeological Science: Reports*, **7**, 432–436
- Ward, I., Merigot, K., McInnes, B.I.A., 2018. Application of quantitative mineralogical analysis in archaeological micromorphology: a Case Study from Barrow Is., Western Australia. *J. Arch. Method and Theory*, **25**, 1, 1–24.

Ward, I., Larcombe, P., Mulvaney, K., Fandry, C., 2013. The potential for discovery of new submerged archaeological sites near the Dampier Archipelago, Western Australia. *Quaternary International*, **308–309**, 216–229.

Ward, I., Veth, P., Prossor, L., Denham, T., Ditchfield, K., Manne, T., Kendrick, P., Byrne, C., Hook, F., Troitzsch, U., 2017. 50,000 years of archaeological site stratigraphy and micromorphology in Boodie Cave, Barrow Island, Western Australia. *J. Archaeological Science: Reports*, **15**, 344–369.

Yokoyama, Y., Lambeck, K., De Deckker, P., Johnson, P., Fifield, L.K., 2000. Timing of the last glacial maximum from observed sea-level minima. *Nature* **406**, 713-716.

Yokoyama, Y., De Deckker, P., Lambeck, K., Johnson, P., Fifield, L.K., 2001a. Sea-level at the last glacial maximum: evidence from northwestern Australia to constrain ice volumes for oxygen isotope stage 2. *Palaeogeography, Palaeoclimatology, Palaeoecology* **165**, 281-297.

Zeanah, D., Basgall, M., Seah, I., 2014. Lithic landscape of Barrow Island: A view from the open scatters. In: Paper Presented at the Society for American Archaeology Conference, Austin, Texas.

Zeanah, D., Basgall, M., Glover, D., Seah, I., current authors and P. Veth in prep A silicified limestone quarry on Barrow Island.

## List of Figures

- Figure 1** **A.** Location of Barrow and Montebello Is. approximately 60 km off the mainland coast of Western Australia. **B.** Location of the major archaeological sites, including (1) Haynes Cave, (2) Noala Cave, (3) calcrete ‘quarry’, (4) Boodie Cave, (5) John Wayne rock shelter, (6) Biggeda Creek, (7) the ‘Chair’, (8) The drill-pad claypan, (9) Bandicoot Bay, (10) claypan 2, (11) red dune, (12) Wapet Landing, and (13) Surf Point. Colour bar is height (m) ASL.
- Figure 2** **A.** Geological map for Barrow Island (centre) (sourced from Ditchfield and Ward 2019, their Fig. 4). Surrounding annotated photos (courtesy of Sacramento University) show mapped locations of artefact scatters from past studies including the Barrow Island Archaeological Project (BIAP) including B. The Quarry, C. close-up of the Quarry, D. Biggeda Creek, E. Loop Beach and F. the airport and Lake Barrow. **Blue dot indicates non-archaeological site locations from this study.**
- Figure 3** Deglacial relative sea-level (RSL) curves for Barrow Island derived from the Glacial Isostatic Adjustment models using the ICE-7G\_NA and ANU-ICE ice models paired with the HetM-LHL140 3-D earth model. The pre-Holocene data are from James et al. (2004), Yokoyama et al. (2000, 2001), whilst the Holocene data (expanded right) are reinterpreted from Twigg and Collins (2010) and May et al. (2015; 2016; 2018). Inferred timings of MWP1A and B are indicated, as are the elevations of the regional horizontal submarine terraces surfaces postulated by Fairbridge (1961; see inset). We have differentiated between pre-Holocene and Holocene marine limiting data because for the pre-Holocene deglaciation the hydro-isostatic effects are likely to be less variable across and along wider areas of the shelf and differences are less important than for the Holocene.
- Figure 4** **A.** Near Map image of BIQ site with sample pit positions and associated OSL ages shown. Note age for BIQ19/2/1 (Shfd20009) was from calcrete and no correction for post-depositional carbonate precipitation for this sample has yet been done. **B.** Grain size profile for dune sands. **C.** Photo showing sharp transition from lighter pink sands to the dark red sands at the base of the dune, and **D.** Photo of section of laminar calcrete.
- Figure 5** **A.** DEM image of Chair (BIC) site (courtesy of Mick O’Leary) with sample pit positions and associated OSL ages shown. **B.** Grain size profile for dune sands (and Gravel Pit). **C.** Photo showing burnt layer in seaward dune, and **D.** Photo showing red sands at base of dune on south side of creek BIC19/1-1 (Site 1), which are dated to have been deposited 120 yrs ago.
- Figure 6** **A.** Photo of quartz-rich red dune, including schematic profile and OSL ages. **B.** Grain size profile of red dune sands compared against dune sands from the north of the island.
- Figure 7** **A.** Near Map image of the drill-pad claypan (Fonz’ gravel pit) site with sample pit positions and associated OSL ages shown. **B.** Grain size profile of gravel pit and other palaeosol sediments on the island. **C.** Profile of gravel pit showing consolidated red sediments (clay/sand) unconformably overlying a gravel-rich unit. Circles indicate fragments of *Terebralia* sp.. **D.** Isolated surface artefacts can be observed adjacent to the gravel pit (scale bar is 5 cm) and may also exist in the spoil heaps.
- Figure 8** **A.** Location of Wapet shell scatters. **B.** Close up image of one of the shell scatters showing single-layer of sparse shells in amongst limestone gravel. Images by DBCA.

- Figure 9** Overview of quartz morphology under PPL (black scale bar is 500  $\mu\text{m}$ ) and microtextures observed using SEM (white scale bar is 200  $\mu\text{m}$ ) for the white (BIQ19-1, BIC19-4) and red (BIQ19-4, BIC19-1, BID) dune sands. The BID sands could arguably be defined as white. Refer text for details.
- Figure 10** Plots of Heavy (HREE) and Light Rare Earth Element (LREE) concentrations against OSL age estimates, showing relative enrichment of LREE and a strong positive correlation with age.
- Figure 11** Simplified reconfiguration of Barrow Island over the last 80 ka using current bathymetric contours to approximate the position of the shoreline at 80 ka, 50 ka and 9 ka respectively. It should be noted, however, that this is only an approximation and does not take into account mobile sediments, changing tidal ranges or other oceanographic drivers.

### List of Tables

- Table 1** Radiocarbon dating of *Terebralia* sp. shell.
- Table 2** Summary of single grain palaeo-dose data and age for the samples from Barrow Is. Where OD was high, finite mixture modelling (FMM) was applied to data resulting in multiple De values and percentage of the dataset they represent. Where significant numbers of saturated grains were measured ages are reported as minimums only. OD values in parenthesis are after outlier De results were removed.
- Table 3 Indicative element ratios determined from ICP data of past and present OSL analyses, with age estimates flagged in red likely to be older than indicated. Highlighted rows show the highest REE abundances.

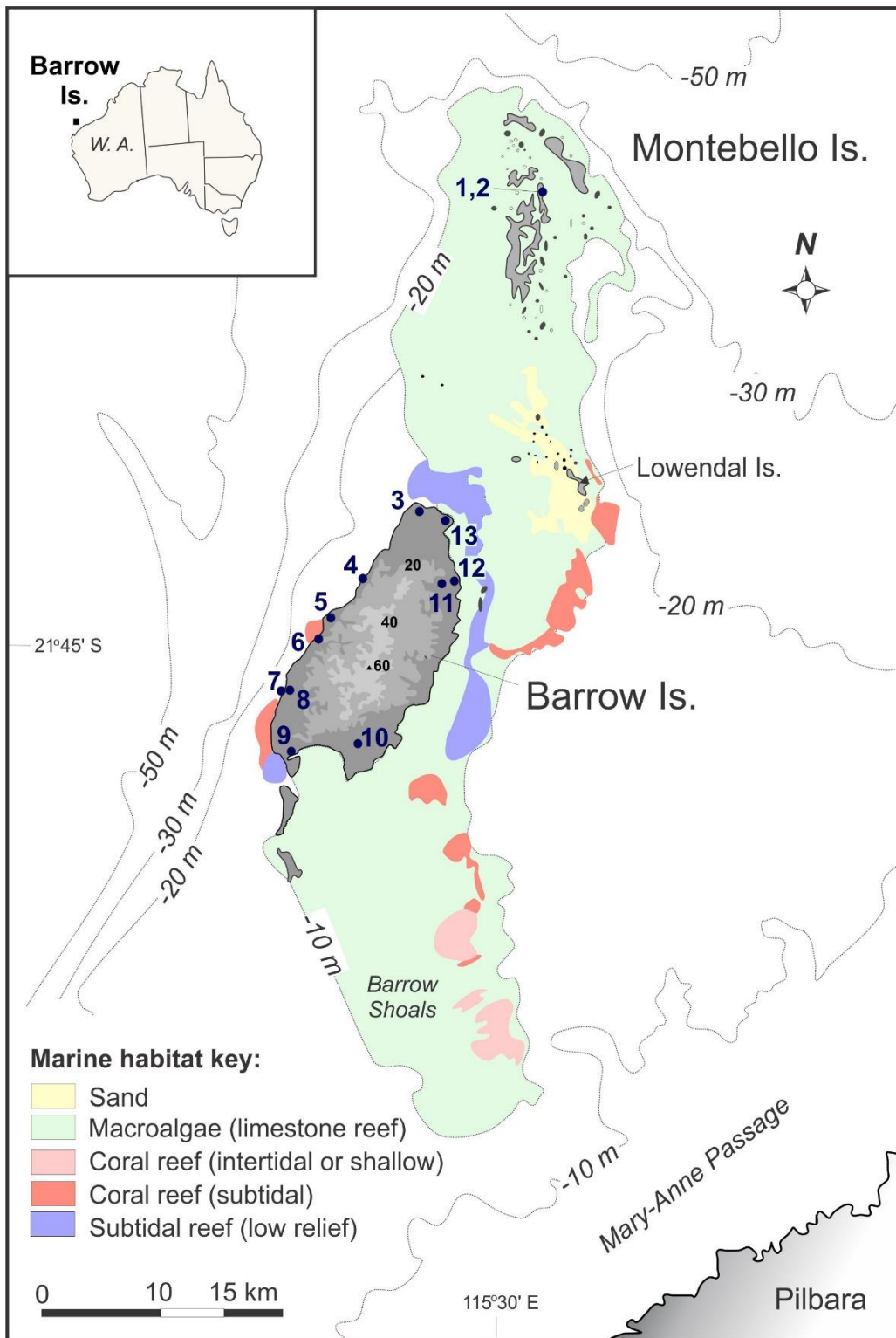


Figure 1 Location of Barrow and Montebello Is. approximately 60 km off the mainland coast of Western Australia, showing major marine habitats (modified from DEC 2017; their Fig. 3) and major archaeological sites: (1) Haynes Cave, (2) Noala Cave, (3) calcrete ‘quarry’, (4) Boodie Cave, (5) John Wayne rock shelter, (6) Biggada Creek, (7) Loop Beach (the Chair), (8) the drill-pad claypan, (9) Bandicoot Bay, (10) Barrow Lake, (11) ‘red dune’, (12) Wapet Landing, and (13) Surf Point. Colour bar is height (m) ASL.

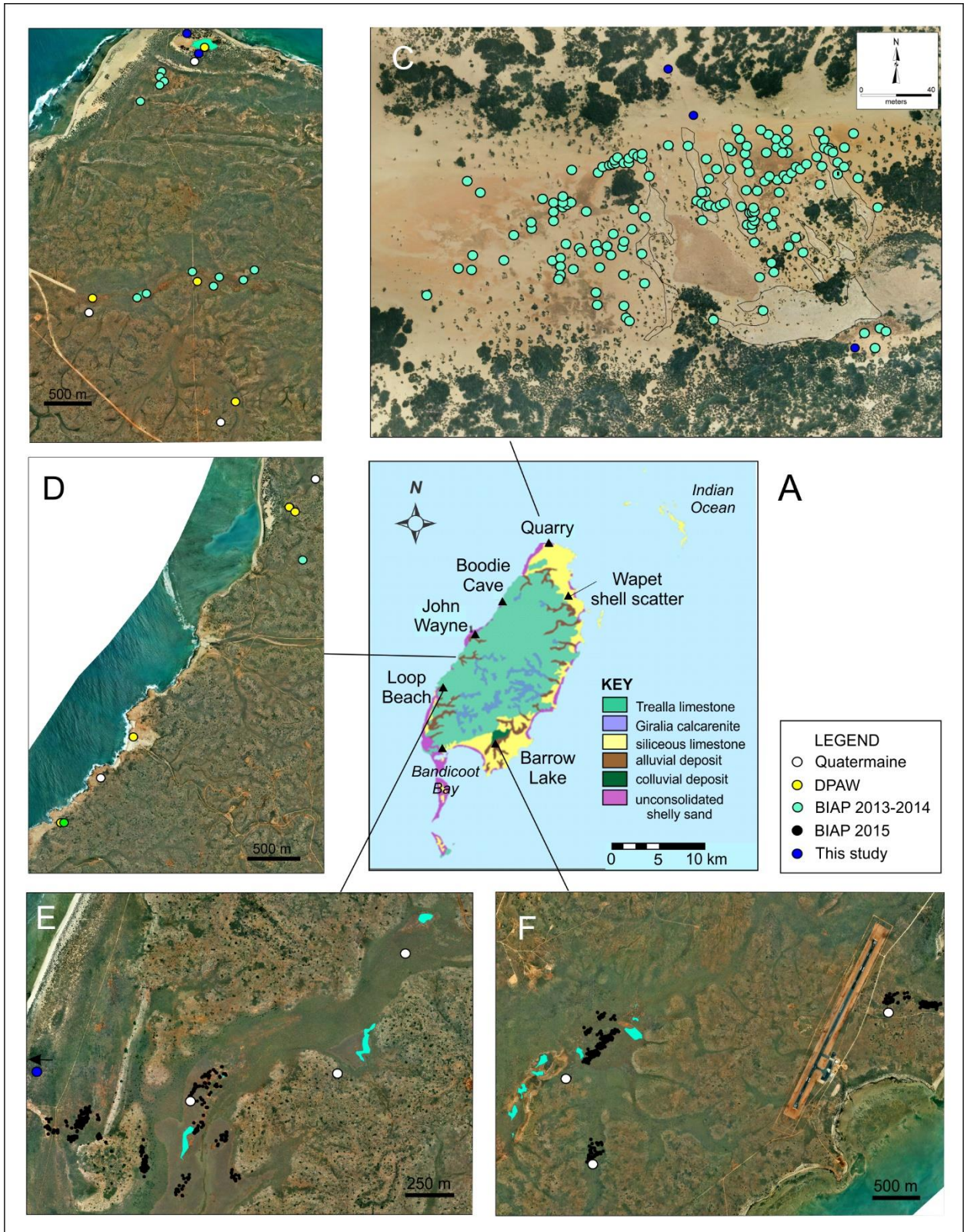


Figure 2 A. Geological map for Barrow Island (centre) (sourced from Ditchfield and Ward 2019, their Fig. 4). Surrounding annotated photos (courtesy of Sacramento University) show mapped locations of artefact scatters from past studies including the Barrow Island Archaeological Project (BIAP) including B. The Quarry, C. close up of the Quarry, D. Biggada Creek, E. Loop Beach and F. the airport and Lake Barrow. Blue dot indicates non-archaeological site locations from this study.

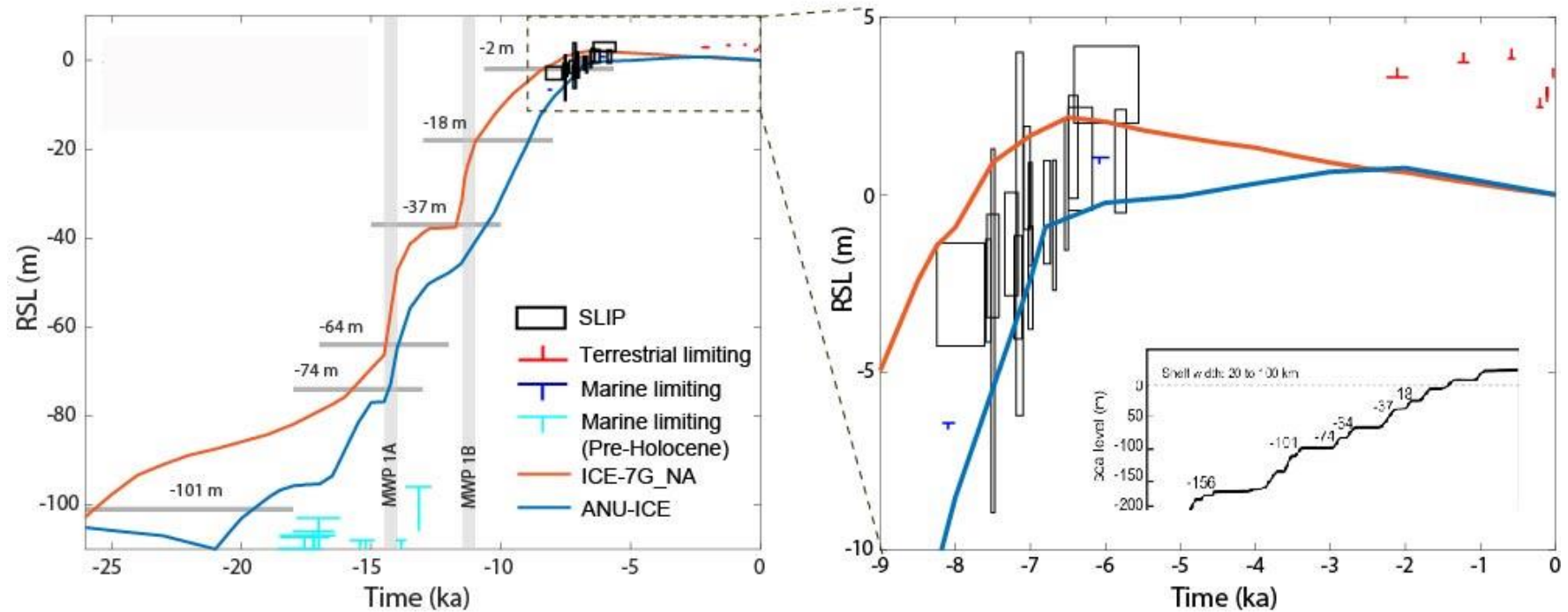


Figure 3 Deglacial relative sea-level (RSL) curves for Barrow Island derived from the Glacial Isostatic Adjustment models using the ICE-7G\_NA and ANU-ICE ice models paired with the HetM-LHL140 3-D earth model. The pre-Holocene data are from James et al. (2004), Yokoyama et al. (2000, 2001), whilst the Holocene data (expanded right) are reinterpreted from Twigg and Collins (2010) and May et al. (2015; 2016; 2018). Inferred timings of MWP1A and B are indicated, as are the elevations of the regional horizontal surfaces postulated by Fairbridge (1961). Inset figure shows the sequence of submarine terraces on the continental margin of Western Australia (after Fairbridge 1961). We have differentiated between pre-Holocene and Holocene marine limiting data because for the pre-Holocene deglaciation the hydro-isostatic effects are likely to be less variable across and along wider areas of the shelf and differences are less important than for the Holocene.

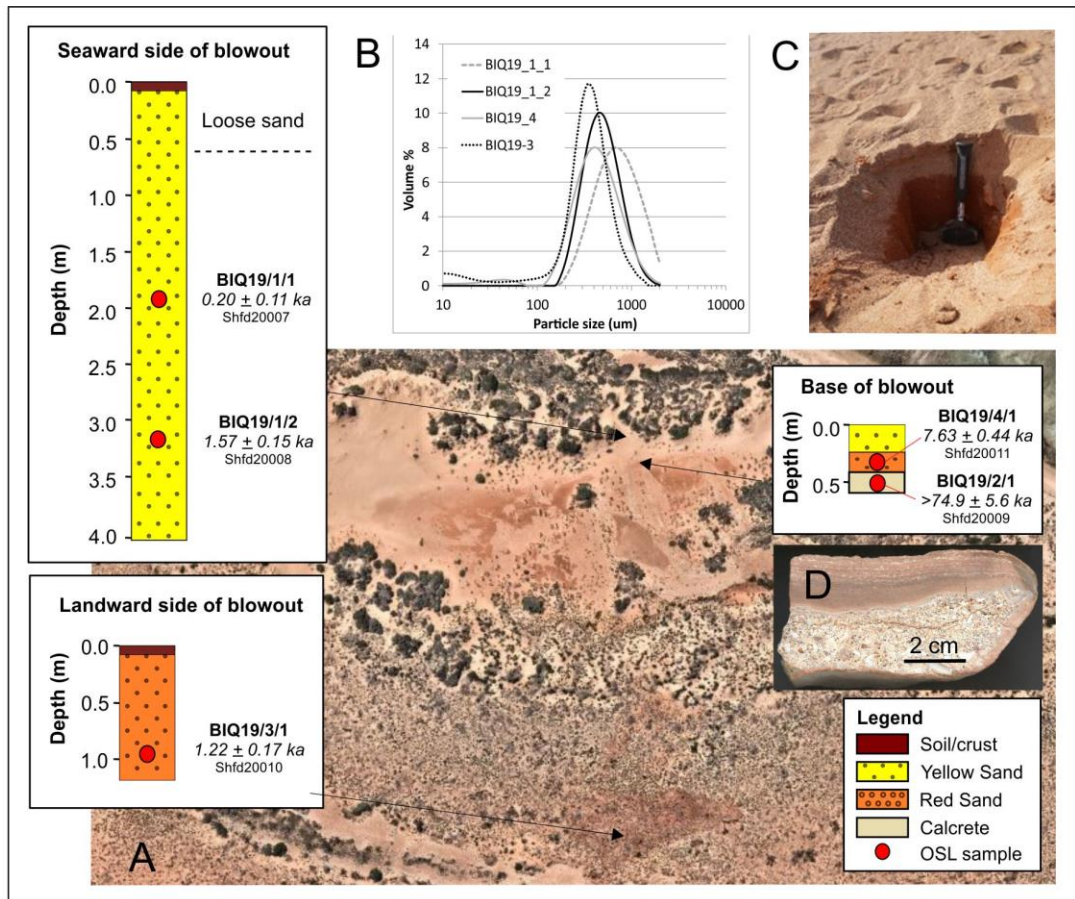


Figure 4 A. NearMap image of BIQ site with sample pit positions and associated OSL ages shown. Note age for BIQ19/2/1 (Shfd20009) was from calcrete and no correction for post-depositional carbonate precipitation for this sample has yet been done, B. Grain size profile for dune sands, C. Photo showing sharp transition from lighter pink sands to the dark red sands at the base of the dune, and D. Photo of section of laminar calcrete.

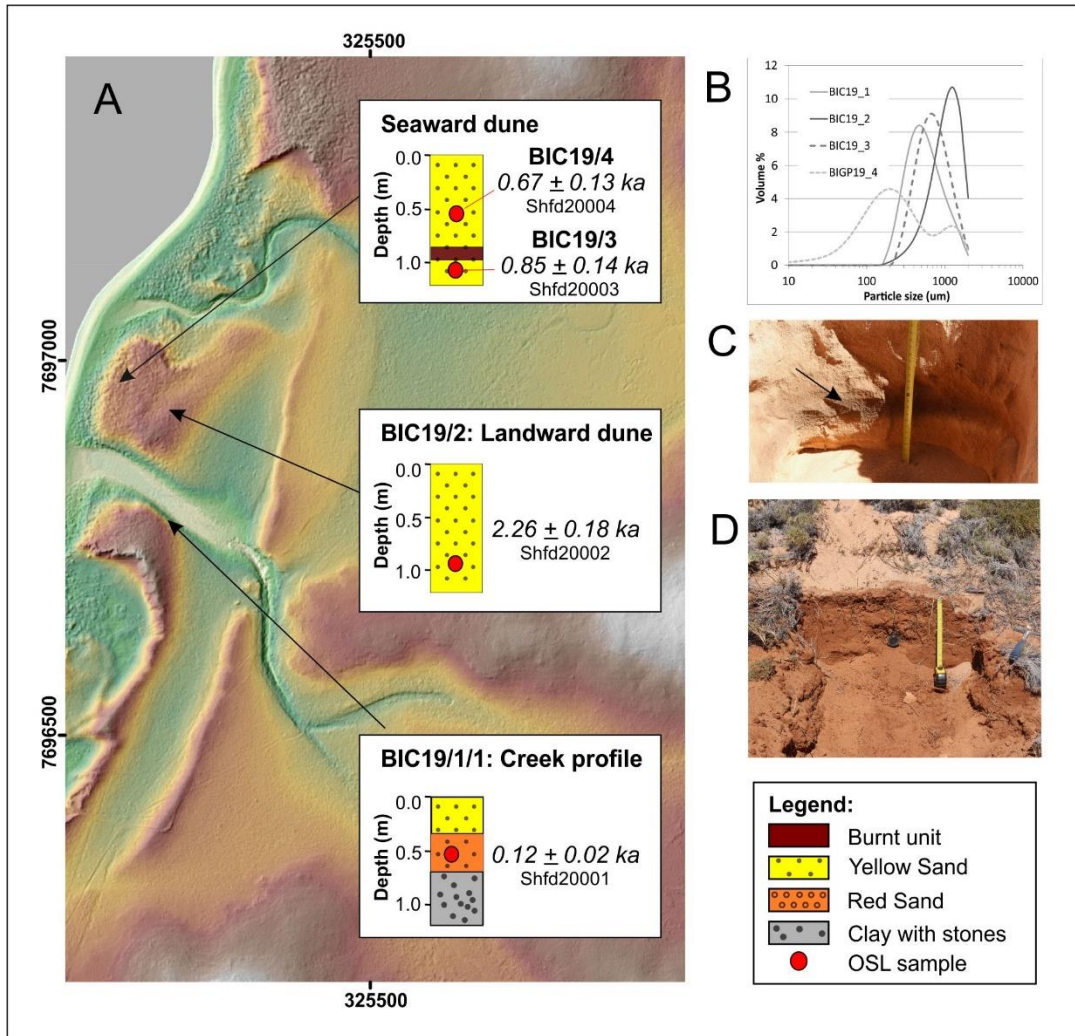


Figure 5 A. DEM image of Chair (BIC) site (courtesy of Mick O’Leary) with sample pit positions and associated OSL ages shown, B. Grain size profile for dune sands (and Gravel Pit), C. Photo showing burnt layer in seaward dune, and D. Photo showing red sands at base of dune on south side of creek BIC19/1-1 (Site 1), which are dated to have been deposited 120 yrs ago.

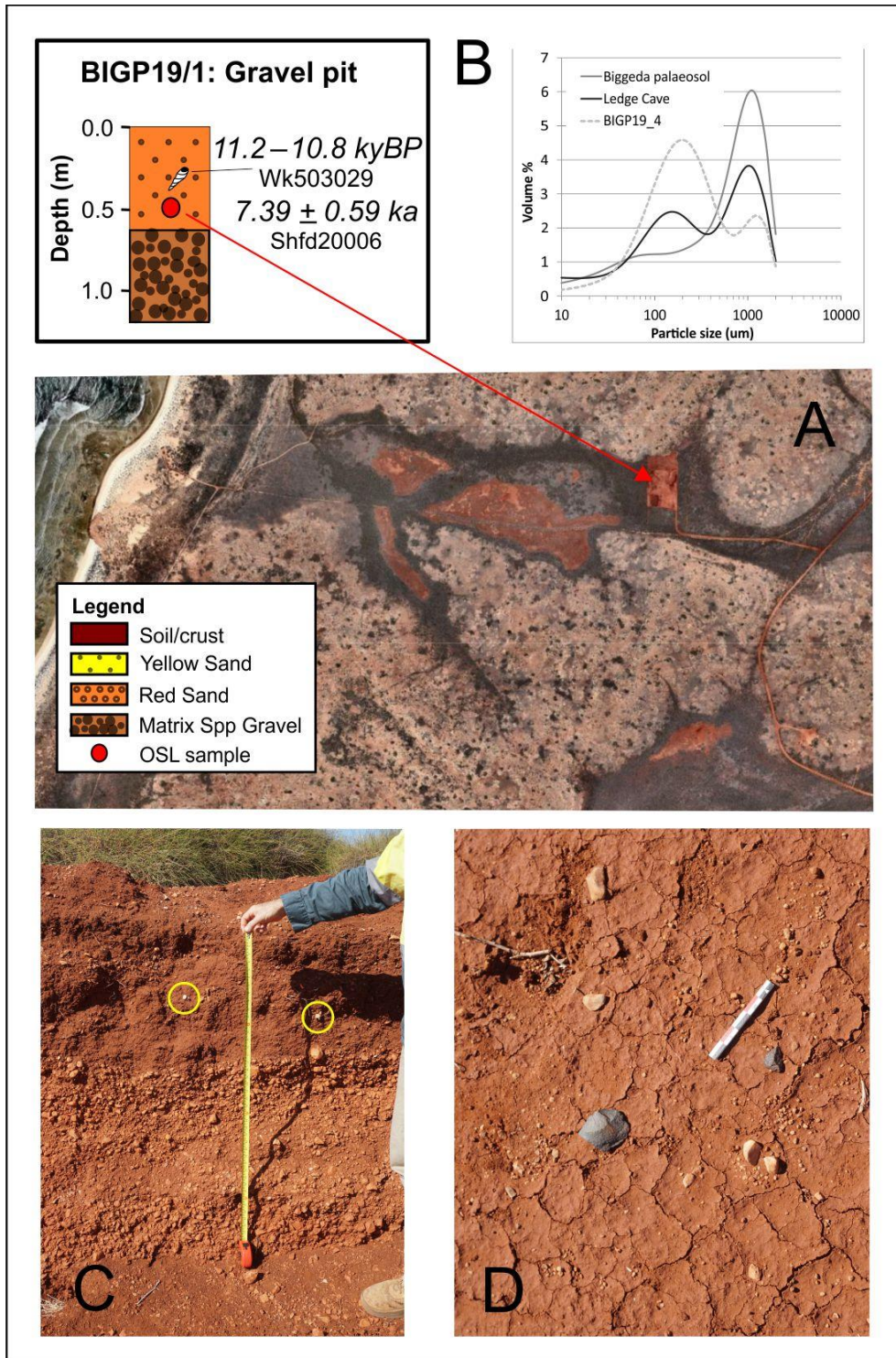


Figure 6 A. Near Map image of the drill-pad claypan (Fonz' gravel pit) site with sample pit positions and associated OSL ages shown. B. Grain size profile of gravel pit and other palaeosol sediments on the island. C. Profile of gravel pit showing consolidated red sediments (clay/sand) unconformably overlying a gravel-rich unit. Circles indicate fragments of *Terebralia* sp.. D. Isolated surface artefacts can be observed adjacent to the gravel pit (scale bar is 5 cm) and may also exist in the spoil heaps.

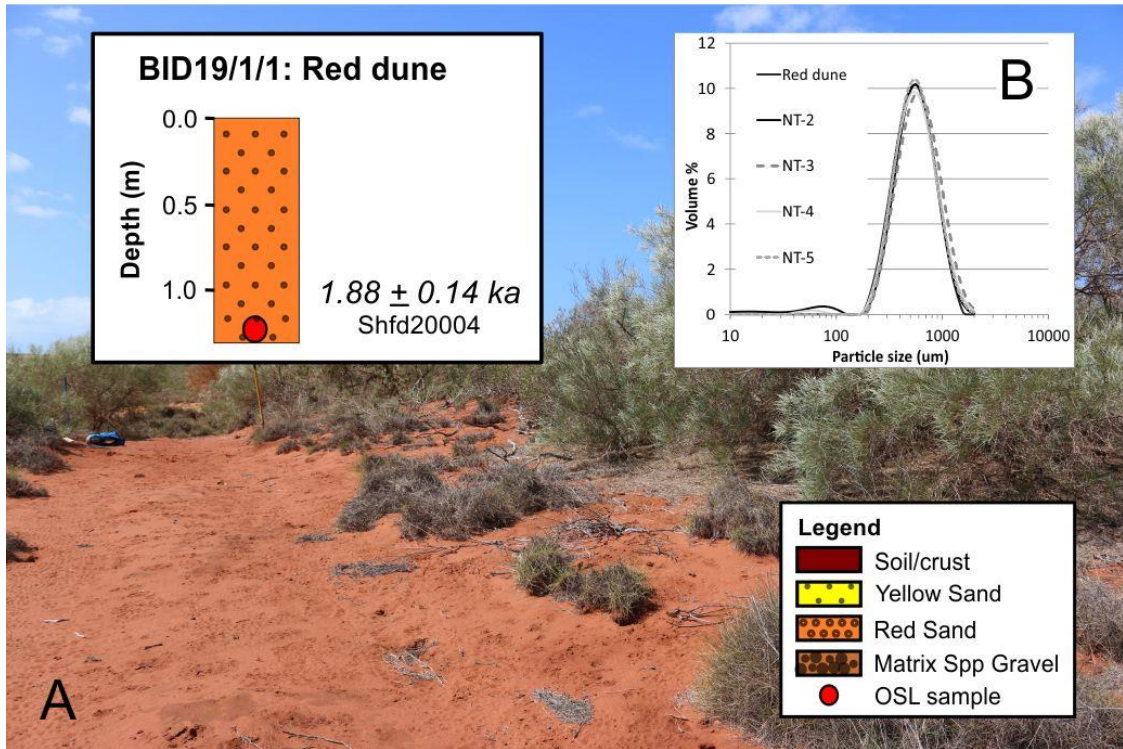


Figure 7 A. Photo of quartz-rich red dune, including schematic profile and OSL ages. B. Grain size profile of red dune sands compared against dune sands from the north of the island.



Figure 8 A. Location of Wapet shell scatters. B. Close up image of one of the shell scatters showing single-layer of sparse shells in amongst limestone gravel. Images by DBCA.

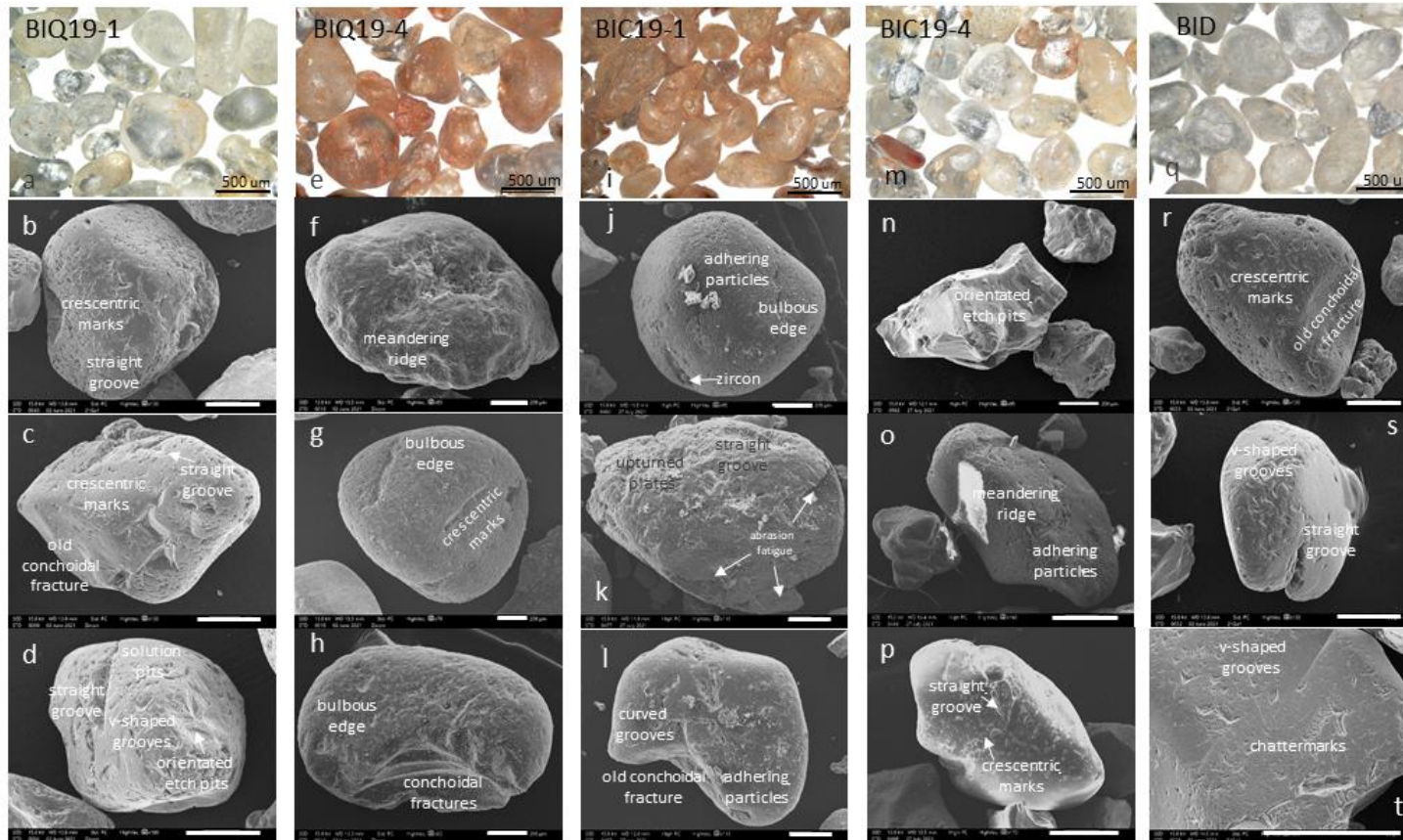


Figure 9 Overview of quartz morphology under PPL (black scale bar is 500  $\mu\text{m}$ ) and microtextures observed using SEM (white scale bar is 200  $\mu\text{m}$ ) for the white (BIQ19-1, BIC19-4) and red (BIQ19-4, BIC19-2, BID) dune sands. Refer text for details.

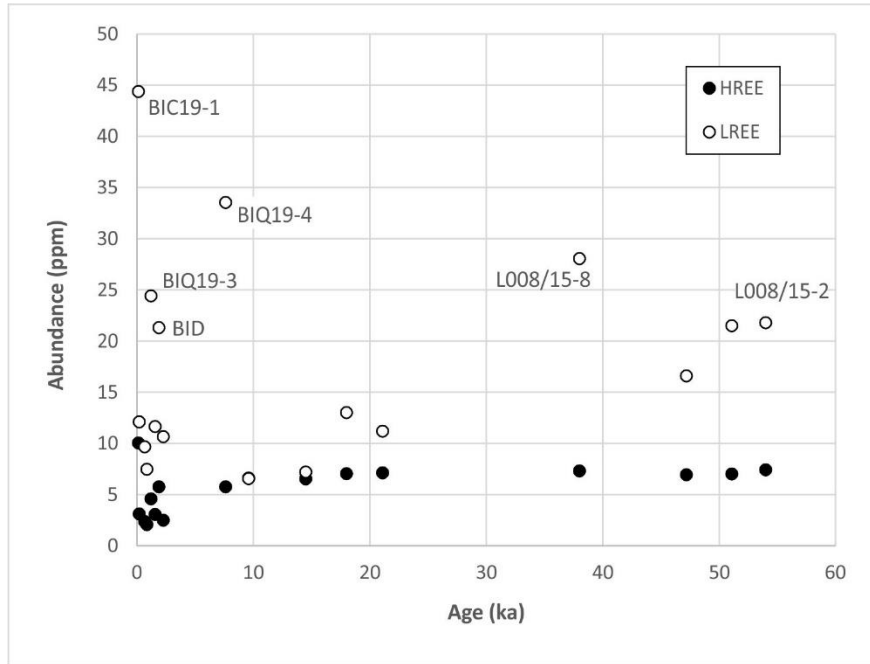


Figure 10 Plots of Heavy (HREE) and Light Rare Earth Element (LREE) concentrations against OSL age estimates, showing relative enrichment of LREE and a strong positive correlation with age. Samples include Barrow Island dunes and Boodie Cave.

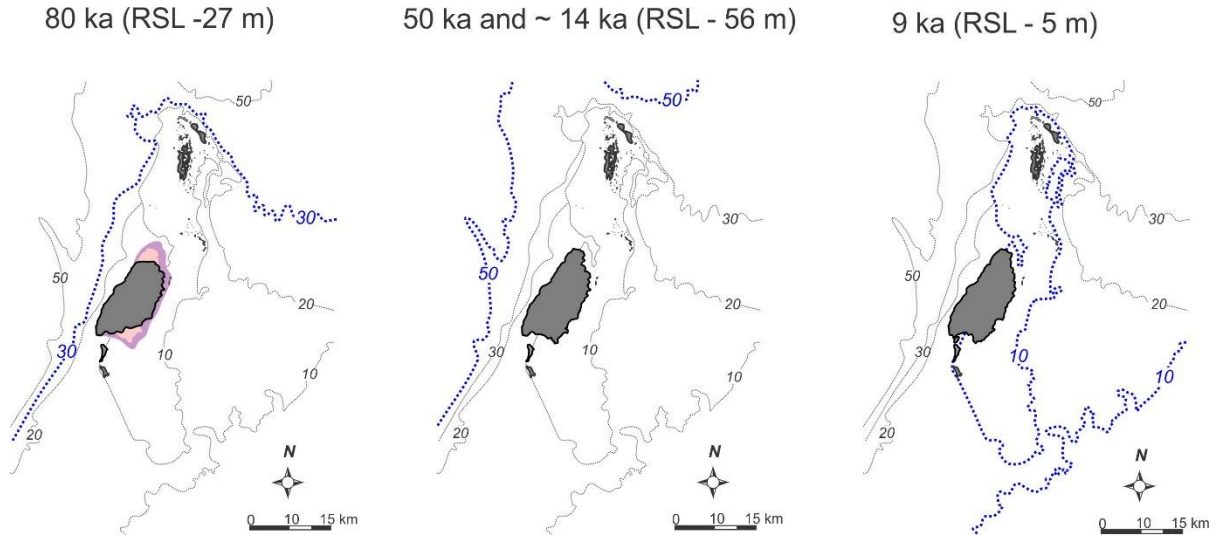


Figure 11 Simplified reconfiguration of Barrow Island over the last 80 ka using current bathymetric contours to approximate the position of the shoreline at 80 ka, 50 ka and 9 ka respectively. It should be noted, however, that this is only an approximation and does not take into account mobile sediments, changing tidal ranges or other oceanographic drivers.

## Tables

Table 1 Radiocarbon dating of *Terebralia* sp. shell.

Location	Lab code	Age uncal. BP	Calibrated age (y BP)
Drillpad (Fonz' gravel pit)	Wk-503029	10,162 ± 33	11,155 – 10,748
Wapet shell scatter	Wk-503030	7232 ± 28	7563 – 7285

Table 2 Summary of single grain palaeo-dose data and age for the samples from Barrow Is. Where OD was high, finite mixture modelling (FMM) was applied to data resulting in multiple De values and percentage of the dataset they represent. Where significant numbers of saturated grains were measured ages are reported as minimums only. OD values in parenthesis are after outlier De results were removed.

Lab Code	Field Ref.	Depth (m)	De (Gy)	Dose rate (µGy/a)	OD (%)	Age (ka)
Shfd20001	BIC19-1	0.2	0.12 ± 0.02	1033 ± 36	129 (0)	0.12 ± 0.02
Shfd20002	BIC19-2	0.95	1.04 ± 0.07	460 ± 18	16 (16)	2.26 ± 0.18
Shfd20003	BIC19-3	1.1	0.38 ± 0.06	446 ± 18	24 (17)	0.85 ± 0.14
Shfd20004	BIC19-4	0.5	0.18 ± 0.02	481 ± 19	40 (0)	0.67 ± 0.13
Shfd20005	BID19-1	1.23	1.57 ± 0.10	834 ± 33	45 (28)	1.88 ± 0.14
Shfd20006	BIGP19-1	0.5	15.01 ± 1.06 (29%)	2031 ± 77	57 (52)	7.39 ± 0.59
			28.75 ± 1.66 (57%)			14.11 ± 0.97
Shfd20007	BIQ19/1-1	1.9	0.11 ± 0.06	548 ± 24	64 (0)	0.02 ± 0.11
Shfd20008	BIQ19/1-2	3.2	0.84 ± 0.07	534 ± 24	59 (19)	1.57 ± 0.15
			16.74 ± 1.24 (22%)	463 ± 17		>36.1 ± 3.0
Shfd20009	BIQ19/2-1	0.1	34.71 ± 2.28 (39%)		109 (105)	>74.12 ± 5.6
			86.7 ± 5.51 (36%)			>187 ± 14
Shfd200010	BIQ19/3-1	0.9	0.97 ± 0.13	797 ± 31	115 (83)	1.22 ± 0.17
Shfd200011	BIQ19/4-1	0.2	5.70 ± 0.25	748 ± 28	34 (28)	7.63 ± 0.44

Table 3 Indicative element ratios determined from ICP data of past and present OSL analyses, with age estimates flagged in red likely to be older than indicated. Highlighted rows show the highest REE abundances.

Sample ID	Age (ka)	Si/Al	Ti/Zr	Rb/Sr	Fe/K	Th/U	Sum LREE	Sum HREE	LREE/HREE
BIC 19-1 (Shfd20001)	0.12 ± 0.02	7.1	0.001	0.009	4.7	2.7	44.4	10.0	4.4
BIC 19-2 (Shfd20002)	2.26 ± 0.18	12.1	0.002	0.001	2.3	0.6	10.7	2.5	4.3
BIC 19-3 (Shfd20003)	0.85 ± 0.14	18.3	0.001	0.001	1.5	0.2	7.5	2.1	3.6
BIC 19-4 (Shfd20004)	0.67 ± 0.13	15.7	0.001	0.001	1.7	0.2	9.7	2.4	4.1
BID 19-1 (Shfd20005)	1.88 ± 0.14	43.5	0.001	1.020	2.1	5.4	21.3	5.8	3.7
BIGP 19-1 (Shfd20006)	14.4 ± 0.97	5.1	0.001	0.597	7.0	7.2	140.0	25.7	5.5
BIQ 19-1-1 (Shfd20007)	0.2 ± 0.11	27.5	0.001	0.002	3.2	0.4	12.1	3.1	3.9
BIQ 19-1-2 (Shfd20008)	1.57 ± 0.15	26.7	0.002	0.001	3.3	0.3	11.6	3.1	3.8
BIQ 19-3-1 (Shfd20010)	1.22 ± 0.17	13.3	0.002	0.004	3.6	0.9	24.4	4.6	5.3
BIQ19-4-1 (Shfd20011)	7.63 ± 0.44	15.7	0.001	0.005	4.0	1.2	33.5	5.8	5.8
L008/15-1	50.0 ± 4.43					5.6	118.4	18.9	6.36
L008/15-2	53.0 ± 4.84					5.7	129.0	19.1	6.7
L008/15-3	17.5 ± 1.52					4.4	72.0	11.4	6.3
L008/15-4	9.58 ± 1.0					3.1	34.6	5.7	6.0
L008/15-5	21.08 ± 1.73					4.1	62.5	9.7	6.4
L008/15-7	47.21 ± 4.00					8.2	90.4	14.5	6.2
L008/15-8	38.09 ± 4.3*					5.3	162.1	24.5	6.6
L008/15-9	14.50 ± 0.31					2.7	36.9	6.7	5.5

\* Original Central Age Model (L008/15-8) = 13.55 ± 1.26 ka

## SUPPLEMENTARY MATERIAL

### S1 Sea-level curve modeling

#### *SI.1 Compilation of sea-level (RSL) data*

Sea-level index points define the discrete position of past RSL in space and time, whereas limiting data points provide an upper (terrestrial limiting data point) or lower (marine limiting data point) bound on the position of RSL (Engelhart et al., 2011; Shennan and Horton, 2002; Shennan et al., 2015). Sea-level index points and limiting data are characterized by the following four fundamental attributes: 1) Geographic location; 2) Age of formation, determined by  $^{14}\text{C}$ , U-series or OSL dating; 3) Elevation of the sample with respect to a contemporary tidal datum; and 4) Relationship of the proxy to sea level. This relationship is known as the ‘indicative meaning’, which describes the central tendency (reference water level) and  $2\sigma$  vertical range (indicative range) of the indicator's distribution relative to tidal levels (Shennan et al., 2015; van de Plassche et al., 1998).

The Holocene RSL record from Exmouth Gulf and the Ashburton Delta consists of 17 index points and 11 limiting data points obtained from coral framework facies ( $n=16$ ) and supratidal tidal flats and sand ridges ( $n=12$ ) (May et al., 2015; May et al., 2016; May et al., 2018; Twiggs & Collins, 2010).

#### *SI.2 Results of ICE-7G\_NA and ANU-ICE models*

The curves (Figure 3) show that RSL rose by  $\sim 103$  m since 26 ka (before present; ICE-7G\_NA) and by  $\sim 110$  m since 21 ka (ANU-ICE). The predicted RSL of ICE-6G\_NA is consistently higher in elevation than that of ANU-ICE until 2.5 ka, when they intersect and become broadly similar in their decrease to the present level. The difference between the curves is highly variable - decreasing from  $\sim 20$  m at 21 ka to  $\sim 8$  m at 15 ka, then increasing to  $\sim 21$  m at 11 ka before they intersect at 2.5 ka. Both curves show a notable signal starting at 14.5 ka corresponding to Meltwater Pulse 1A (MWP1A), when RSL rises rapidly by  $\sim 20$  m over  $\sim 500$  years (e.g., Lambeck et al., 2014; Peltier et al, 2015). The ICE-7G\_NA model shows a significant MWP1B signal starting at  $\sim 11.5$  ka, when RSL rises rapidly by  $\sim 12$  m over  $\sim 500$  years (Figure 9, Roy & Peltier 2017), but the ANU-ICE model does not show an obvious MWP1B signal (Lambeck et al., 2014). The ICE-7G\_NA model reaches present sea level (RSL of 0 m) at  $\sim 7.7$  ka and is followed by a mid-Holocene RSL highstand of  $\sim +2.2$  m at 6.5 ka, while the ANU-ICE model reaches present sea level at  $\sim 5$  ka BP and has a RSL highstand of  $\sim +0.8$  m at 2 ka.

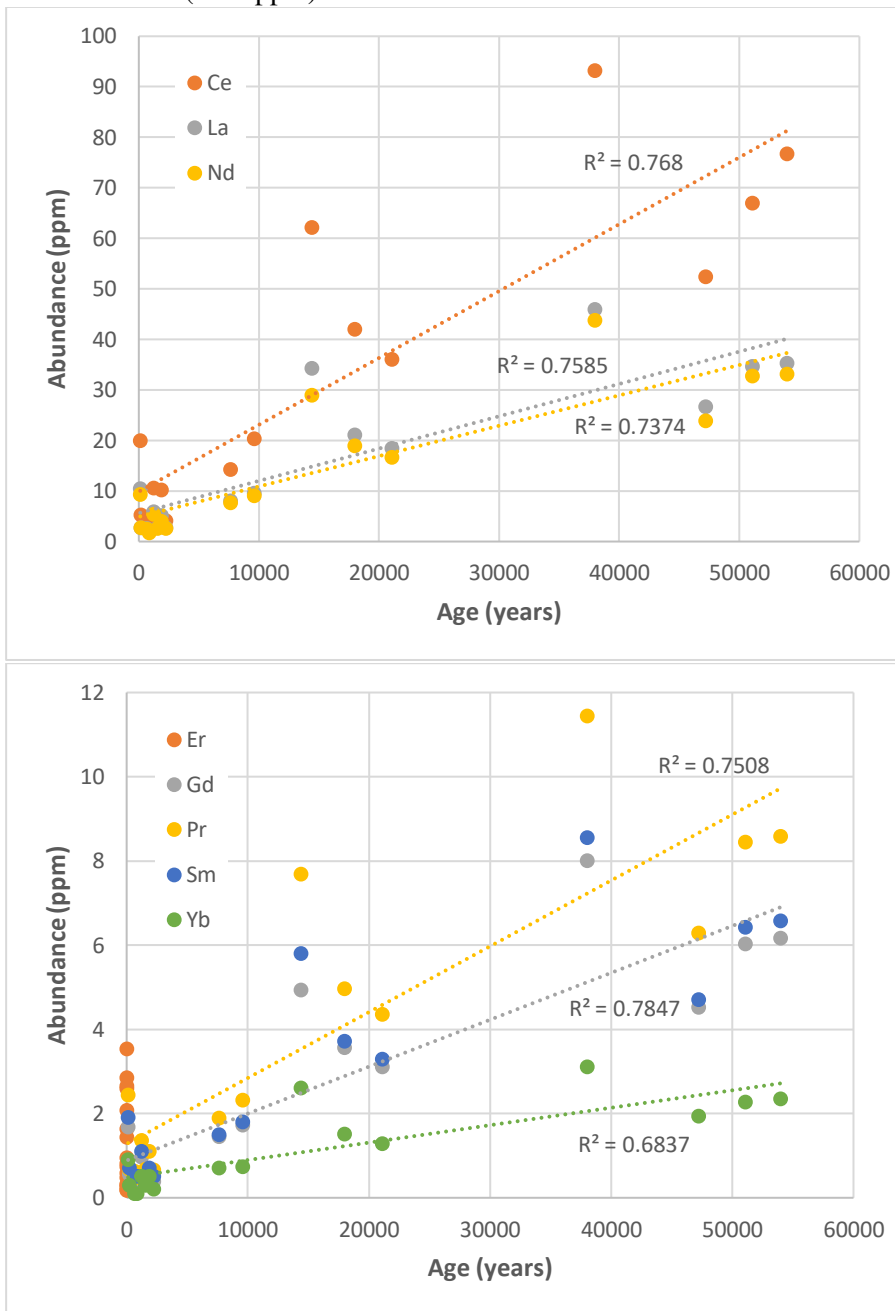
Whilst the depths of Fairbridge’s (1961) proposed stillstands at 37, 18 and 2 m below modern sea level are broadly consistent with the deceleration of RSL rise from the ICE-7G\_NA model, and proposed stillstands at 101, 74 and 2 m below modern sea level match the deceleration of RSL rise from the ANU-ICE model (Figure 3), other proposed stillstands do not match. The tidal range will have changed through time, forming a confounding factor. Mismatches may also reflect relatively weak cementation of coastal and subtidal formations that are thus vulnerable to subsequent reworking

and/or that the submarine terraces were formed by older falling stages of sea level during the glaciation period. Further, some palaeoshoreline features may have been buried beneath younger sediments - as an example, O'Leary et al. (2020) argued that a variety of palaeo-shoreline features at 70 – 75 m below modern sea level and evident in 3D seismic data NW of Barrow Island were likely formed in the period 57 – 29 ka, with the key caveat that the features had not yet been dated.

Coral data broadly agree with the highstand timing predicted by ICE-7G\_NA, although ICE-7G\_NA predictions are higher and ANU-ICE predictions are lower than the RSL evolution indicated by the data. At least in part, this is likely to reflect that data from coral cores can only indicate a minimum level for RSL, and corals were likely in catch-up mode at this time anyway (Larcombe & Woolfe, 1999) because of the prior period of rapid rise in RSL. Both model predictions are consistent with late Holocene limiting data that place RSL below ~2 m from ~ 3 ka to present, but the data themselves are few.

Whether the post-highstand fall in RSL contained oscillations (e.g., as postulated by Baker et al., 2005) or was more smooth (e.g., Searle & Woods, 1986; Colins et al., 2006) is of little relevance for the purposes of this paper, and whilst there are other sea-level data points for the region, including soft sediment deposits such as swash deposits, their precise meaning in terms of sea level is generally unclear (Lewis et al., 2013). Overall, both models and the existing field data, mostly of which is located above -25 m, can be used to inform our interpretation of past changes in coastal environments around Barrow Island.

Figure S1 Plots of Rare Earth (Lanthanide) element (REE) concentrations against OSL age estimates, showing a strong positive correlation in all elements. For clarity, plots are separated for those REE with (top) high abundance (up to 100 ppm), and (bottom) low abundance (< 12 ppm).



## S2 U-series age estimates

Supplementary Table S1 U-series age estimates of calcrete basal laminae sampled from the Quarry.

Sample name	238U [V]	2SE	230Th (cps)	2SE	Th230/U238	±2SE	U234/U238	±2SE	Th232/U238 _uncorr	±2SE	Calculated age (ka BP 1950)	±2s (abs)	Initial 234U/ 238U AR	±2s (abs)
<b>Basal_laminae1_2</b>	0.01636	0.00015	6.29	0.28	1.12E-05	5.40E-07	6.72E-05	2.90E-06	5.03E-09	1.00E-10	<b>82.934</b>	<b>8.122</b>	1.2811	±0.062
<b>Basal_laminae1_3</b>	0.015673	0.000065	5.51	0.24	1.02E-05	4.90E-07	7.13E-05	2.70E-06	3.29E-09	2.20E-11	<b>66.261</b>	<b>5.576</b>	1.3581	±0.056
<b>Basal_laminae1_4</b>	0.014757	0.000081	5.56	0.27	1.09E-05	5.70E-07	6.88E-05	2.60E-06	3.95E-09	5.20E-11	<b>76.215</b>	<b>7.133</b>	1.3119	±0.055
<b>Basal_laminae1_5</b>	0.014125	0.000076	5.54	0.27	1.15E-05	5.90E-07	6.79E-05	2.90E-06	3.19E-09	3.30E-11	<b>84.030</b>	<b>8.527</b>	1.2981	±0.062
<b>Basal_laminae2_1</b>	0.013706	0.000056	4.85	0.25	1.03E-05	5.80E-07	6.88E-05	2.30E-06	3.93E-09	5.60E-11	<b>71.092</b>	<b>6.513</b>	1.3075	±0.048
<b>Basal_laminae2_2</b>	0.014964	0.000087	5.49	0.27	1.07E-05	5.70E-07	6.87E-05	2.80E-06	4.55E-09	4.40E-11	<b>75.102</b>	<b>7.254</b>	1.3087	±0.059
<b>Basal_laminae2_3</b>	0.014332	0.000067	5.18	0.25	1.07E-05	5.70E-07	6.74E-05	3.30E-06	4.16E-09	5.20E-11	<b>77.013</b>	<b>8.195</b>	1.2810	±0.070
<b>Basal_laminae2_4</b>	0.013544	0.000067	4.89	0.24	1.07E-05	5.70E-07	7.03E-05	3.20E-06	3.98E-09	5.40E-11	<b>72.464</b>	<b>7.226</b>	1.3421	±0.067
<b>Basal_laminae2_5</b>	0.012158	0.000056	4.24	0.23	9.91E-06	5.80E-07	6.94E-05	2.90E-06	4.59E-09	1.30E-10	<b>66.350</b>	<b>6.563</b>	1.3165	±0.060

Supplementary Table S2

Summary of dosimetry related data for OSL age dating.

Lab Code	U (ppm)	Th (ppm)	K (%)	Rb (ppm)	D <sub>cosmic</sub> ( $\mu$ Gy/a)	Moisture (%)	Beta Dose rate ( $\mu$ Gy/a)	Gamma Dose rate ( $\mu$ Gy/a)
Shfd20001	1.3	3.5	0.3	17.2	191 $\pm$ 10	2.7	445 $\pm$ 30	376 $\pm$ 191
Shfd20002	0.82	0.5	<0.01	2.5	172 $\pm$ 9	1.1	147 $\pm$ 14	126 $\pm$ 6
Shfd20003	0.87	0.2	<0.01	1.6	168 $\pm$ 8	1.6	146 $\pm$ 14	117 $\pm$ 6
Shfd20004	0.97	0.2	<0.01	1.8	183 $\pm$ 9	2.5	156 $\pm$ 15	127 $\pm$ 7
Shfd20005	0.41	2.2	0.4	15.3	171 $\pm$ 9	0.4	396 $\pm$ 30	250 $\pm$ 11
Shfd20006	1.59	11.4	0.7	46.6	183 $\pm$ 95	4.2	941 $\pm$ 63	855 $\pm$ 41
Shfd20007	1.31	0.5	<0.01	3.8	151 $\pm$ 8	2.7	203 $\pm$ 20	177 $\pm$ 9
Shfd20008	1.38	0.4	<0.01	3.4	127 $\pm$ 6	2.6	210 $\pm$ 21	180 $\pm$ 10
Shfd20009	0.65	0.8	<0.01	3.9	194 $\pm$ 10	1.0	133 $\pm$ 12	122 $\pm$ 6
Shfd20010	1.41	1.2	0.2	9.9	173 $\pm$ 9	1.1	344 $\pm$ 26	261 $\pm$ 12
Shfd20011	1.28	1.5	0.2	11.9	153 $\pm$ 8	3.9	323 $\pm$ 24	253 $\pm$ 12

Supplementary Table S3

Summary of ICP data from past and present OSL analyses, with age estimates flagged in red likely to be older than indicated. Highlighted rows show the highest REE abundances.

Sample ID	Age (ka)	Al	Fe	Mn	Ti	K	Zr	U	Ce	Dy	Er	Eu	Gd	Hf	Ho	La	Lu	Nd	Pr	Sm	Tb	Th	Tm	U	Yb
BIC 19-1 (Shfd20001)	0.12 ± 0.02	1.31	1.41	140	0.12	0.3	146	1.3	19.9	1.66	0.95	0.43	1.67	4	0.34	10.4	0.13	9.3	2.44	1.9	0.23	3.5	0.15	1.3	0.9
BIC 19-2 (Shfd20002)	2.26 ± 0.18	0.19	0.23	26	0.02	<0.1	11	0.82	4.1	0.41	0.24	0.11	0.39	1	0.08	2.7	0.05	2.6	0.65	0.5	0.07	0.5	0.05	0.82	0.2
BIC 19-3 (Shfd20003)	0.85 ± 0.14	0.12	0.15	17	0.01	<0.1	13.8	0.87	2.7	0.24	0.17	0.1	0.33	1	0.07	2	0.05	1.7	0.47	0.5	0.05	0.2	0.05	0.87	0.1
BIC 19-4 (Shfd20004)	0.67 ± 0.13	0.14	0.17	20	0.01	<0.1	8.5	0.97	3.3	0.35	0.18	0.14	0.47	1	0.09	2.6	0.05	2.5	0.63	0.5	0.06	0.2	0.05	0.97	0.1
BID 19-1 (Shfd20005)	1.88 ± 0.14	0.69	0.82	79	0.08	0.4	98	0.41	10.2	0.71	0.48	0.19	0.68	3	0.15	5.1	0.06	4	1.1	0.7	0.11	2.2	0.07	0.41	0.5
BIGP 19-1 (Shfd20006)	14.4 ± 0.97	4.58	4.9	557	0.39	0.7	302	1.59	62.1	4.71	2.85	1.2	4.93	8	0.99	34.3	0.39	28.9	7.69	5.8	0.78	11.4	0.4	1.59	2.6
BIQ 19-1-1 (Shfd20007)	0.2 ± 0.11	0.2	0.32	49	0.01	<0.1	10.9	1.31	5.2	0.6	0.32	0.13	0.55	1	0.14	2.7	0.05	2.7	0.67	0.7	0.09	0.5	0.05	1.31	0.3
BIQ 19-1-2 (Shfd20008)	1.57 ± 0.15	0.18	0.33	47	0.02	<0.1	8.6	1.38	5	0.55	0.29	0.15	0.6	1	0.12	2.7	0.05	2.6	0.68	0.5	0.09	0.4	0.05	1.38	0.3
BIQ 19-3-1 (Shfd20010)	1.22 ± 0.17	0.61	0.71	93	0.05	0.2	26.6	1.41	10.6	1	0.58	0.25	0.96	1	0.22	5.8	0.08	5.3	1.36	1.1	0.14	1.2	0.09	1.41	0.5
BIQ19-4-1 (Shfd20011)	7.63 ± 0.44	0.72	0.79	98	0.05	0.2	43.2	1.28	14.2	1.19	0.74	0.34	1.45	1	0.26	8	0.1	7.6	1.89	1.5	0.21	1.5	0.1	1.28	0.7
L008/15-1	50.0 ± 4.43								66.9	4.81	2.59	1.34	6.03	3.29	0.92	34.7	0.34	32.7	8.45	6.43	0.86	11.3	0.38	2.01	2.27
L008/15-2	53.0 ± 4.84								76.7	4.89	2.64	1.37	6.16	3.19	0.94	35.3	0.35	33.2	8.58	6.57	0.87	12.5	0.40	2.17	2.34
L008/15-3	17.5 ± 1.52								42.0	2.93	1.63	0.82	3.55	1.83	0.58	21.0	0.22	18.9	4.96	3.71	0.51	6.23	0.25	1.41	1.50
L008/15-4	9.58 ± 1.0								20.3	1.44	0.81	0.39	1.73	1.08	0.28	9.58	0.11	8.98	2.32	1.80	0.25	3.44	0.13	1.11	0.74
L008/15-5	21.08 ± 1.73								36.1	2.57	1.43	0.72	3.10	1.42	0.51	18.5	0.19	16.7	4.35	3.28	0.45	4.82	0.22	1.17	1.28
L008/15-7	47.21 ± 4.00								52.4	3.72	2.08	1.00	4.52	2.35	0.73	26.6	0.28	23.9	6.28	4.70	0.65	10.1	0.33	1.23	1.93
L008/15-8	38.09 ± 4.3*								93.1	6.41	3.53	1.77	7.99	3.64	1.24	45.9	0.46	43.7	11.4	8.54	1.13	15.1	0.53	2.82	3.11
L008/15-9	14.50 ± 0.31																								

\* Original Central Age Model (L008/15-8) = 13.55 ± 1.26 ka